8-2022

Evaluation of the Geothermal Potential of the Camas Prairie, South-Central Idaho

Connor J. Smith
Utah State University

UtahStateUniversity
MERRILL-CAZIER LIBRARY

EVALUATION OF THE GEOTHERMAL POTENTIAL OF THE CAMAS

PRAIRIE, SOUTH-CENTRAL IDAHO

By

Connor J. Smith

A thesis submitted in partial fulfillment

of the requirements for the degree

of

MASTER OF SCIENCE

in

Geology

Approved:

Thomas Lachmar, Ph.D. Major Professor	John Shervais, Ph.D. Committee Member
William Doucette, Ph.D. Committee Member	D. Richard Cutler, Ph.D. Interim Vice Provost of Graduate Studies

UTAH STATE UNIVERSITY

Logan, Utah

2022

ABSTRACT

Evaluation of the Geothermal Potential of

the Camas Prairie, Southcentral Idaho

by

Connor J. Smith, Master of Science

Utah State University, 2022

Major Professor: Dr. Thomas E. Lachmar
Department: Geosciences

The Snake River Plain (SRP) is a volcanic province, which trends across southern Idaho

and has an abundance of hot springs and wells that contain high temperature waters. The eastern

portion of the SRP tracks plate movement over the stationary Yellowstone hotspot and

experiences high heat transfer as a result. Based on the favorable geothermal characteristics of

high permeability, active magmatic emplacement, and the presence of high temperature surface

waters and a cold-water aquifer, the SRP was selected for exploration by the predecessor of this

project, the Snake River Geothermal Drilling Project (Project Hotspot). Three areas across the

SRP were drilled under Project Hotspot and have been listed in order of their geothermal

potential from highest to lowest: Mountain Home, Kimama, and Kimberly.

Recent exploration for geothermal resources in the SRP used a Play Fairway Analysis

(PFA) approach. PFA integrates geophysical, geological, and geochemical data into a statistical

framework to locate regions with high geothermal potential. The PFA revealed an area in the

Camas Prairie, Idaho, located north of the Project Hotspot wells, exhibiting favorable geothermal conditions. To validate this geothermal assessment, the Camas Prairie was selected for drilling.

An exploration borehole (USU Camas-1) was advanced using rotary methods to ~491.3 m (1,612 ft) below ground surface (bgs) in October 2018. In the fall of 2019, the hole was extended and cored to a total depth of ~618 m (2,028.5 ft) bgs.

Cuttings display alteration at the depth drillers reported encountering a productive zone at ~347.5 m (1,140 ft) with inflow of hot water. X-ray diffractometry (XRD) of core shows that alteration is present throughout the lower section of the borehole as well. Geophysical logs of SP, resistivity, conductivity, gamma ray, and delta t reacted to the productive zone and further validate its presence. The maximum groundwater temperature measured was 80.3°C at ~354 m (1,160 ft). The artesian flow rate measured in July 2019 was ~0.7 L/s. Soon thereafter the head declined to a level below the surface. A section of USU Camas-1 that accepted cold injected water centered at a depth of ~357.5 m (1,173 ft) demonstrates the presence of a permeable zone. The transmissivity of this permeable zone was ~0.1-0.4 cm^2/s (9-36 ft^2/d).

Plotting the major ion concentrations of the USU Camas-1 water sample on a Piper (1944) diagram show that USU Camas-1 is sodium-bicarbonate type, like most Project Hotspot and other Camas Prairie water samples. The USU Camas-1 water sample exhibits more negative values of δ^{18}O and δ^{2}H than local waters sampled at higher elevations in the Mount Bennet Hills to the south and the Soldier Mountains to the north. Plotting these values on a global meteoric water line (GMWL) shows that the groundwater is influenced by meteoric waters and is consistent with local trends in δ^{18}O and δ^{2}H established by previous spring and well samples.

Results of various geothermometers suggest that the reservoir in which the USU Camas-1 water sample equilibrated has a temperature of ~125°C. Based on these data, as well as the temperatures and depths of other wells in the vicinity, it appears as if the geothermal fluids originate along the fault along the north margin of the Mount Bennett Hills and then flow horizontally north along the Pothole fault. The USU Camas-1 well is an adequate low-temperature geothermal resource, but its reservoir does not appear to reach temperatures sufficient for generating electricity efficiently.

(93 pages)

PUBLIC ABSTRACT

Evaluation of the Geothermal Potential of

the Camas Prairie, Southcentral Idaho

The area studied in this thesis was assessed based on the analysis of a water sample collected from the exploratory well USU Camas-1. The water sample was characterized and compared to other water samples collected and analyzed during a previous phase of this project according to its water chemistry.

Lithologic, geophysical, and temperature logs were also used to assess the study area. The depth sensitive data was analyzed to determine the characteristics of the formation as they relate to the favorable parameters of a geothermal resource, those being permeability of the subsurface, heat, and the presence of a clay seal.

The analyses suggest that USU Camas-1 falls short of being a high-temperature resource capable of generating electricity efficiently. However, temperatures are high enough for the resource to be developed as a low-temperature asset that could be utilized to heat buildings in the area.

ACKNOWLEDGMENTS

CONTENTS

LIST OF TABLES

LIST OF FIGURES

INTRODUCTION

Significance

Assessing the geothermal potential of the Camas Prairie of south-central Idaho has significant implications for both local and global communities regarding sustainability and economics. The urgency for the planet to adopt renewable resources, such as geothermal energy, grows as the climate crisis intensifies. Sanderson and O'Neil (2020) estimate that delaying climate change mitigation efforts increases the cost by 0.3-0.9 trillion dollars annually, and that in order to halt global warming to no more than 2°C, as per the Paris global average temperature goal, humanity will need to reduce emissions by 50% in the next 15 years and reach net-zero emissions by 2060. Monetary incentives of harnessing the Camas Prairie's geothermal potential also exist on the local scale, for discovering geothermal fluids with relatively high temperatures on the Camas Prairie would provide the surrounding area with new jobs and stimulate the economy once the resource was developed. The utility of geothermal is two-fold: aid in reaching growing energy needs, while simultaneously lowering emissions through the replacement of fossil fuel infrastructure.

Geothermal energy is a renewable resource with two categories of application: high-temperature and low-temperature. Systems with reservoir temperatures ≥150°C are categorized as high-temperature geothermal, while systems with reservoir temperatures below this threshold are categorized as low-temperature geothermal. High-temperature systems can generate electricity, and low-temperature systems are mainly used to heat buildings. Communities near the Camas Prairie could benefit from both types of geothermal resources.

The Snake River Plain (SRP), a topographically low volcanic region located just south of Camas Prairie that covers most of southern Idaho, has shown great promise as a geothermally

rich area for its high-temperature waters and association with the Yellowstone hotspot. The

SRP's magmatic association, the relatively high temperatures of surface waters recorded in the

area, and the presence of a cold aquifer potentially masking warmer fluids spurred Shervais et al.

(2016) to explore the SRP for geothermal plays. This project was known as the Snake River

Geothermal Drilling Project (Project Hotspot) and is the predecessor of the current project.

Project Hotspot identified three areas worthy of geothermal exploration on the SRP: Mountain

Home, Kimberly, and Kimama (Figure 1). Of these, Mountain Home boasted the greatest

potential for development as a high-temperature geothermal resource. Kimama showed

intermediate potential, and Kimberly showed the lowest potential (Freeman, 2013; Shervais et

al., 2013).
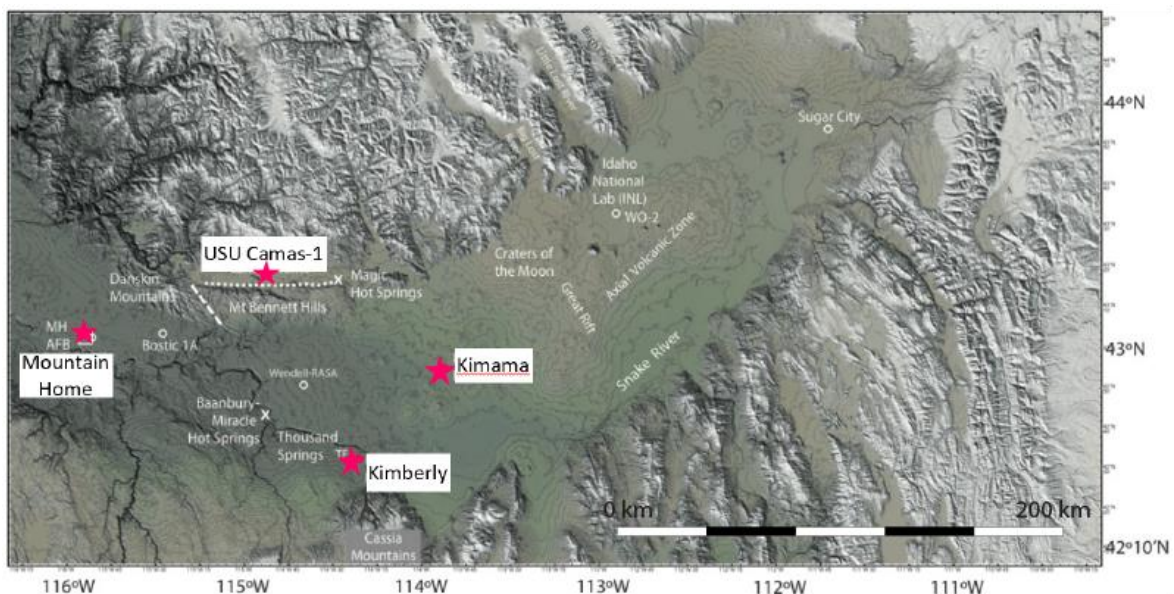
Figure 1. Location map of the SRP, the location of the phase three USU Camas-1 well and the
Snake River Geothermal Drilling Project (SRGDP) phase two wells, are marked with red stars
(adapted from Shervais et al., 2015).

By adapting the Play Fairway Analysis (PFA), an exploratory method used in the

petroleum industry for locating areas with a high likelihood of containing oil, Shervais et al.

(2016) developed the Geothermal Play Fairway Analysis (GPFA) to identify the best plays for

geothermal exploration on the SRP. The Camas Prairie was identified by Shervais et al. (2018) as a favorable location for exploration via the GPFA (Figure 1), and was selected to validate the model and fill in data gaps from the previous drilling efforts of Project Hotspot. The Camas Prairie is a representative geothermal play for the central SRP. Funded by the U.S. Department of Energy (DOE), the drilling of the exploratory USU Camas-1 well on the Camas Prairie commenced in the fall of 2018.

The drilling site of the USU Camas-1 well was selected at a point on the Camas Prairie that rests ~610 m (2,000 ft) above the projected confluence of two major fault systems. This highly permeable network was suspected of being a productive hydrothermal zone, thus making it a good location to drill (Glen et al., 2017). The USU Camas-1 well was first drilled to a depth of ~491.3 m (1,612 ft) below ground surface (bgs) via rotary methods. Then, after a ten-month hiatus during which the DOE allocated residual funds to the project, the USU Camas-1 well was cored to a total depth (TD) of ~618.3 m (2,028.5 ft) bgs. Drilling and wireline logging were carried out by the U.S. Geological Survey (USGS) Research Drilling unit.

Project Goals

This project uses the lithology and mineralogy of the core, geophysical data, temperature data, the results of an injection test, and water chemistry, specifically major cations and anions and isotopes of oxygen and hydrogen, to assess the potential for geothermal energy production of the Camas Prairie.

The lithology and mineralogy of important rock core intervals were determined to clarify the tectonic and volcanic origins of the system in finer detail. Magmatic associations and

hydrothermal alteration also are taken into consideration when appraising the area's geothermal potential, and may aid in clarifying the area's paleo-metasomatic temperatures.

Geophysical data (conductivity, resistivity, natural gamma ray, spontaneous potential (SP), and delta t) were collected. Resistivity and conductivity data are used to gain a better understanding of the formation's permeability, porosity, and saturation. The SP data are used to determine the salinity of the formation and the clay content of permeable beds. Gamma ray data are used to evaluate the lithology of the formation.

Temperature logs were conducted on subsurface fluids present in the USU Camas-1 well. These logs are used to determine the geothermal gradient of the system and to project at what depth the highest temperature will occur. This will establish whether it is economically feasible to develop the region as either a high- or low-temperature geothermal resource.

Injection tests are used to determine the hydraulic properties of a borehole. Three shut-in tests were conducted, two following the rotary drilling and the other following the coring of the USU Camas-1 well. The pressure and depth data gathered during the second of the first two tests is used to estimate the hydraulic properties of the well.

The water chemistry of the USU Camas-1 well is compared to the chemistry of the three nearby wells drilled for Project Hotspot and analyzed by Freeman (2013). Cation concentrations are used in calculations to estimate a reservoir temperature. A reservoir temperature estimate is useful in providing an approximate maximum temperature of the system. The temperatures calculated using geothermometry are distinct from, and expected to be greater than, the fluid temperatures measured directly in the well. The fluids present in the well, in theory, were exhumed from the reservoir at depth and migrated upwards to depths accessible via drilling.

During upward migration, these geothermal fluids lost some of the heat retained while in the geothermal reservoir. Therefore, it is important to review both direct temperature measurements as well as those calculated using cation signatures of water samples.

Anion concentrations are used in tandem with the cation concentrations to calculate the alkalinity of the geothermal fluids. Stable isotope data has been plotted relative to the global meteoric water line (GMWL). This plot helps to determine the degree of mixing between meteoric precipitation and the geothermal fluid.

Location

The location of the USU Camas-1 well site is shown on Figure 1. The Camas Prairie, an east-west trending graben nested between the Mount Bennett Hills to the south and the Soldier Mountains to the north, rests north of the SRP and near its axis (Figure 1). Exact GPS coordinates and elevation of the well site are N43.29950, W114.90826 and 1,544 m, respectively, with an error of +/- 3 m.

BACKGROUND

Geologic and Hydrologic Setting

The Camas Prairie lies to the north of the SRP, an arcing, topographically low volcanic province that exhibits high heat flow associated with the Yellowstone hotspot, and trends from eastern Oregon to western Wyoming (Blackwell, 1989). The SRP is bounded by normal faults to the west and remains unbound to the east. The western Snake River Plain (WSRP) was first distinguished from the eastern Snake River Plain (ESRP) based on this discovery by Malde (1959). The WSRP is a tectonic rift basin, while its eastern counterpart is a topographic low associated with the Basin and Range Province (Parsons et al., 1998) (Figure 2). According to Blackwell and Richards (2004) there is significant heat flow beneath the SRP aquifer.
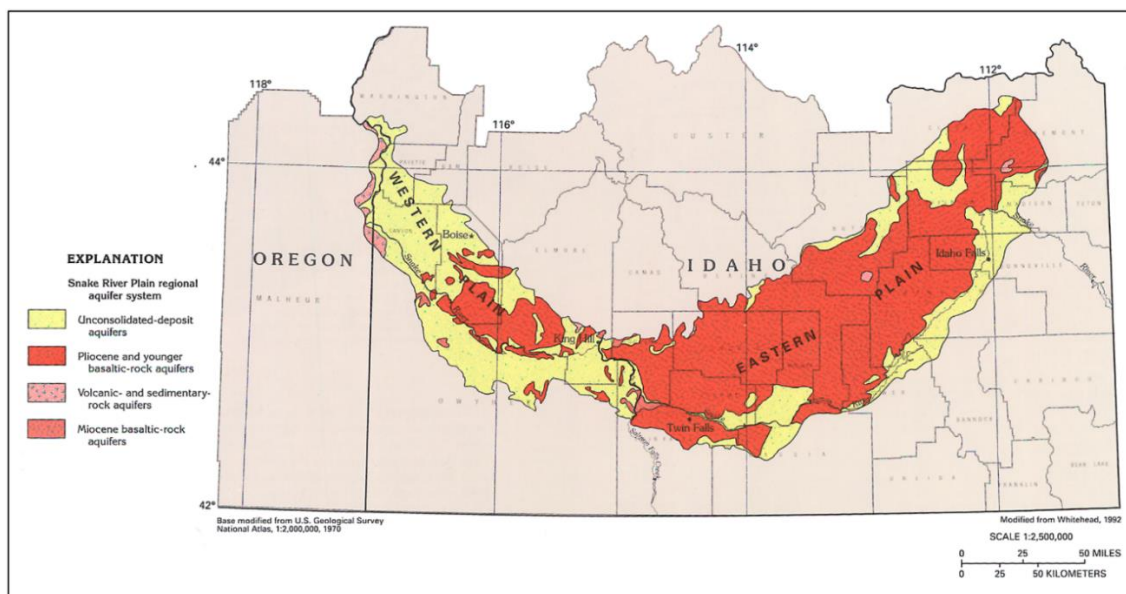
Figure 2. Map showing the extents of the WSRP and ESRP and the aquifers associated with them (adapted from Whitehead, 1992.)

As the North American plate shifts to the SW (average azimuth of 232.4 ± 6.3°), the ESRP moves at an average velocity of 2.5 cm per year and the mafic plume that provides heat to the Yellowstone Hotspot remains in place (Chadwick et al., 2007). In much the same way that

the islands of Hawaii trace plate movement over the plume responsible for their creation, the

succession of calderas and altered rhyolite along the ESRP track traces the tectonic shift of the

North American plate over the Yellowstone Hotspot (Smith and Braile, 1994; Smith et al., 2009),

as shown in Figure 3. Between ~16 and 17 Ma, the area now referred to as the ESRP rested

above the Yellowstone Hotspot and was subjected to its eruptions (Smith and Braile, 1994).

These explosive eruptions are the source of rhyolite associated with the ESRP today.
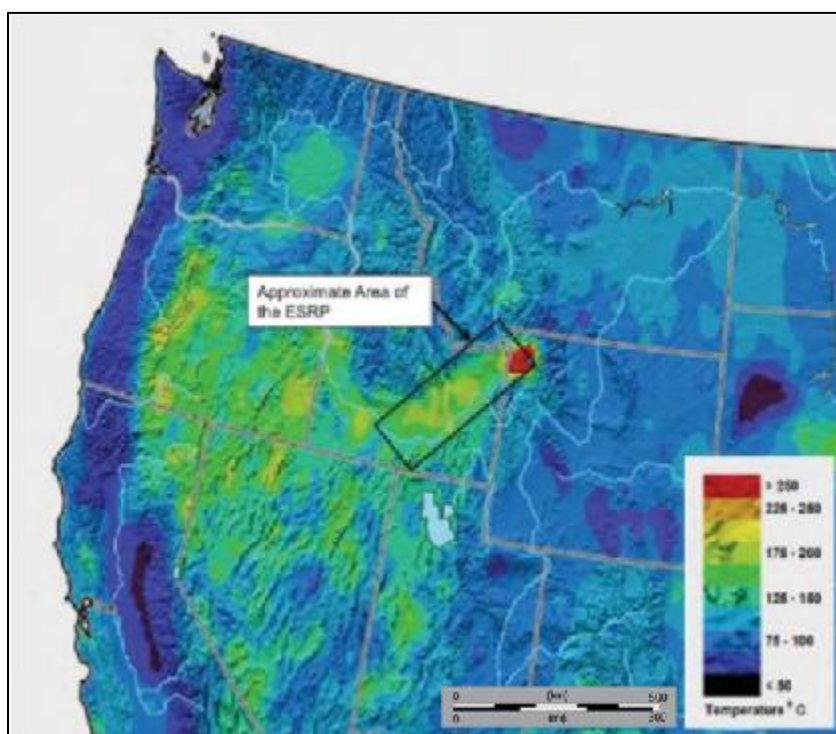
Figure 3. Map of the western United States showing the approximate temperatures of the
subsurface at a depth of ~3 km, (adapted from McLing et al., 2014). The area of the ESRP,
bracketed in black, resides along the track of the Yellowstone Hotspot.

Following the explosive caldera-forming events of the ESRP, basaltic magmas, such as

those that compose the Mount Bennett Hills, were emplaced during a period of cooling and

contraction. In the ESRP, basaltic volcanism proliferated during this period (Blackwell, 1989).

In the Camas Prairie, lava flows obstructed the basin's outlet during the Pliocene

resulting in the deposition of poorly sorted lacustrine sediments and Quaternary valley fill and

alluvium along its eastern margin into the Pleistocene. The grain size of the valley fill ranges from coarse at the base of the Soldier Mountains to fine near the center of the prairie. The source of these sediments is the Idaho batholith along the Camas Prairie's northern margin. The depth to basement bedrock is relatively shallow on the Camas Prairie, varying between 30.5 m (100 ft) near the eastern outlet of the prairie and ~305 m (1,000 ft) near the USU Camas-1 well site (Walton, 1962).

The Atlanta lobe of the Idaho batholith, bounding the northern margin of the Camas Prairie, is composed of Late Cretaceous (67-83 Ma) biotite granodiorite and granite (Kiilsgaard and Lewis, 1985; Gaschnig et al., 2011). The basement of the Camas Prairie consists of this formation as well as what Lewis and Kiilsgaard (1991) refer to as an Eocene pink granite. Intruding into the Atlanta lobe and outcropping to the south of it, the Challis suite of the Mount Bennett Hills are Eocene in age (44-51 Ma) and composed mostly of basalt, dacite, and andesite (Clemens and Wood, 1993; Gaschnig et al., 2011). The rhyolite in the Mount Bennett Hills is Miocene in age (9-10 Ma) and is part of the Idavada series (Honjo, 1990; Shervais et al., 2002). Fractures in these formations allow for groundwater to flow through otherwise impermeable igneous rocks (Walton, 1962).

The Camas Prairie is a highly faulted area; WNW-trending faults occupy the area east of the Pothole fault, while the area to the west of the Pothole fault is occupied by a set of faults that strike NNW (Shervais et al., 2017). Offset at the Pothole volcanic crater rim dates the local faulting event to less than 700 ka. The convergence of fault systems on the Camas Prairie is a part of what makes the area an outstanding candidate for geothermal exploration (Shervais et al., 2016).

Shallow aquifers of the Camas Prairie are unconfined and occur in lacustrine sediments and valley-fill supplied by the Idaho batholith along the Camas Prairie's northern flank, while geothermal fluids at depth experience head levels, at times, great enough for flow to reach the surface. Interbedded clayey sand and sandy clay act as confining layers for these pressurized fluids.

Geothermal Energy

A geothermal resource requires the presence of three characteristics: a permeable network, a heat source, and a seal. High permeability allows groundwater in a system to percolate down to, and interact with, hot rocks at depth. Once the waters have been heated, high permeability in the subsurface allows the now geothermal fluids to rise to shallow and accessible depths. A heat source is perhaps the most obvious component of a geothermal system besides water. The term "geothermal" refers to heat sourced from the Earth. Either a radiogenic or primordial source of heat is required to heat the system. A primordial heat source is regulated by the residual heat of the Earth's formation, while a radiogenic source is regulated by the radioactive decay of isotopes (Strutt, 1906; Holmes, 1925). Typically, the source of heat comes from a magmatic body. According to Blackwell (1989), the anomalously high heat flow associated with the SRP is due to the penetration of mafic magmas into the upper crust. This is supported by the anomalously high ^{3}He/^{4}He ratios of the Camas Prairie (Dobson et al., 2015; Neupane et al., 2017). Finally, a cap or seal of clay to act as an insulator for the heat is required for the system. A clay seal also acts as an impermeable plane beneath which the geothermal fluids will spread out laterally (Cumming, 2016).

As depth increases, so too, generally, do subsurface temperatures. The rate at which the temperature of geothermal fluids increases, per a steady increase in depth, is referred to as the

system's geothermal gradient. A geothermal gradient of 50°C/km would mean that for every kilometer gained in depth, a subsequent and gradual rise in temperature of ~50°C would occur. Geothermal wells are typically economical in the range of 3 to 4 km bgs.

As stated previously, there are two categories of geothermal: low-temperature, otherwise known as direct, geothermal and high-temperature, or indirect, geothermal. Low-temperature requires a minimum fluid temperature of 20°C, and is used for heating buildings and industrial purposes. High-temperature geothermal resources have a minimum fluid/steam temperature of 150°C and may be used to generate electricity. Indirect geothermal can harness the heat from dry or flash steam (efficient at >180°C), or liquids that steam when mixed with high temperature geothermal fluids to spin a turbine and thereby generate electricity in a method known as binary steam (efficient in the range of 107-180°C) (Fazal and Kamran, 2021).

Low-temperature geothermal systems may be used to heat buildings, to melt snow, for agricultural applications, such as dehydrating crops, and for small-scale power generation. Using passive geothermal heating reduces energy needed from other heat sources, so it is both economical and environmentally savvy to heat buildings in this way. Heating greenhouses is an example of a low-temperature geothermal application. An example of a low-temperature facility would be the Chevilly-L'Haÿ-Villejuif geothermal heat plant located in Paris, France.

The electricity produced by high-temperature geothermal is an unequivocally useful commodity of the modern world and one that society currently underutilizes. The Earth's largest high-temperature geothermal resource is located in California and known as The Geysers. This single source has a generation capacity of ~1,000 Megawatts-electric (MWe). A recent assessment of geothermal resources estimated that the power capacity of geothermal in the U.S. was >2,500 MWe, while the potential of identified and unidentified geothermal systems were

9,057 Mwe and 30,033 Mwe, respectively (Williams et al., 2008). The assessment also estimated that by creating geothermal reservoirs in areas that experience high heat flow but lack permeability, the U.S. could generate 517,800 MWe.

As it stands, countries around the planet are slowly adopting renewable energy sources in a bid to combat climate change. Securing high-temperature geothermal resources for electricity and low-temperature geothermal resources for heating where possible in the US will aid the country in reaching its goal of becoming a net-zero emissions state by 2050.

Previous Work

Prior to the GPFA, Project Hotspot sought to elucidate the interactions between mafic plumes and cratonic lithosphere at continental hotspots. Most studies involving hotspots are done at sea. Investigations into cratonic hotspots are few by comparison, and not much is known about how mafic plumes affect the geochemistry of the lithosphere and vice versa (Shervais et al., 2013). As part of Project Hotspot, three areas were selected for drilling exploratory wells (Figure 1). Project Hotspot was funded by the DOE, and drilling was conducted by Drilling, Observation, and Sampling of Earth's Continental Crust (DOSECC), a nonprofit that works with the International Continental Drilling Program (ICDP).

Of the three regions drilled for Project Hotspot, the most promising for geothermal power was the Mountain Home Air Force Base. The Mountain Home well boasts the greatest geothermal gradient of the three at ~ 73°C/km. The maximum temperature recorded at the Mountain Home well was 140°C. Kimama boasts temperatures and gradients of intermediate favorability; a maximum temperature of 59.3°C, and gradients of 5.5°C/km in the upper section and 88.9°C/km in the lower section. The least promising area according to gradient and

maximum temperature recorded was Kimberly, with gradients of 15.1°C/km in the upper section and 5°C/km in the lower section, and a maximum recorded temperature of 57.3°C. Geothermometry results were most favorable for Mountain Home, with a calculated reservoir temperature of 138.8°C, and Kimama, with a calculated reservoir temperature between 124.5 and 138.6°C, while the lowest calculated reservoir temperature was that of Kimberly, at 112.9°C (Freeman, 2013).

Elevated shallow and surficial temperatures of surface waters recorded on the Camas Prairie have made it an area of geothermal interest for decades. The Camas Prairie is a highly permeable region with a convoluted extensional fault system located near a sill complex of layered mafic intrusions circulating geothermal fluids at depth (Nielson and Shervais, 2017). These features, in accordance with the presence of a clay seal, as suggested by magnetotellurics (Glen et al., 2017), high surficial and shallow well temperature measurements (Mink, 2010), anomalously high ^{3}He/^{4}He ratios measured from water samples (Shervais et al., 2016; Glen et al., 2017), the presence of relatively young volcanics, and elevated reservoir temperatures of up to 200°C estimated by Neupane et al. (2017) give the Camas Prairie a high favorability score as per the GPFA, and thus make it an area of interest for geothermal exploration. The high demand for electricity at Sun Valley, ID, a ski town located ~60 km NE of the wellsite, make the Camas Prairie an ideal candidate for geothermal exploration as well (Figure 4).

Under the GPFA, Shervais et al. (2016) created risk layers for the three necessary parameters a geothermal system must possess: high permeability, high heat flow, and presence of a seal. By weighting the spatial data for each risk layer and stacking them in ArcGIS, Shervais et al. (2016) produced a composite common risk segment (CCRS) map (Figure 5). The CCRS map assigns favorability scores to cells representing a location's "risk" or likelihood of containing

high-temperature geothermal fluids. The GPFA was executed in three phases to fill in data gaps

of the existing model and enhance the resolution of promising areas.
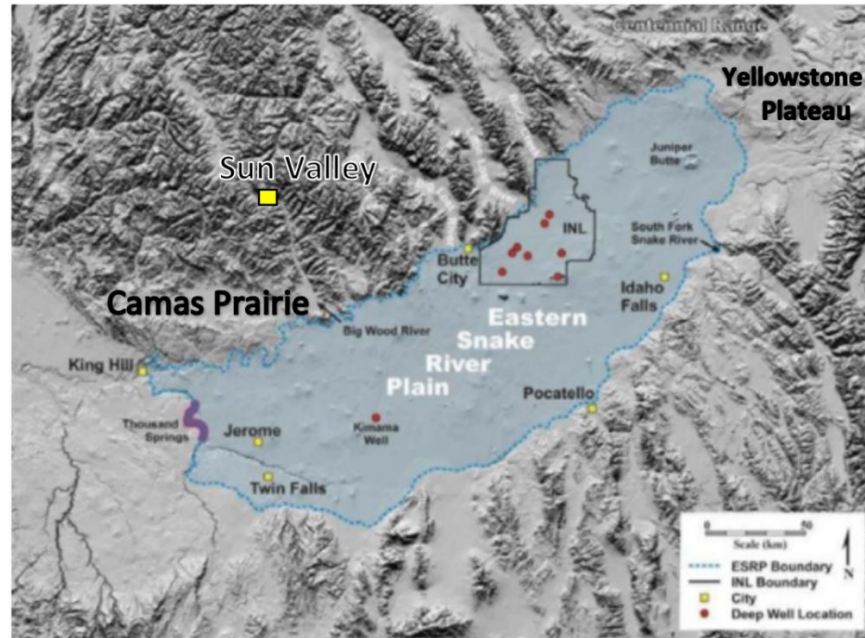
Figure 4. Map of the ESRP showing the location of the Camas Prairie in relation to Sun Valley, represented by a yellow square (adapted from McLing et al., 2014).
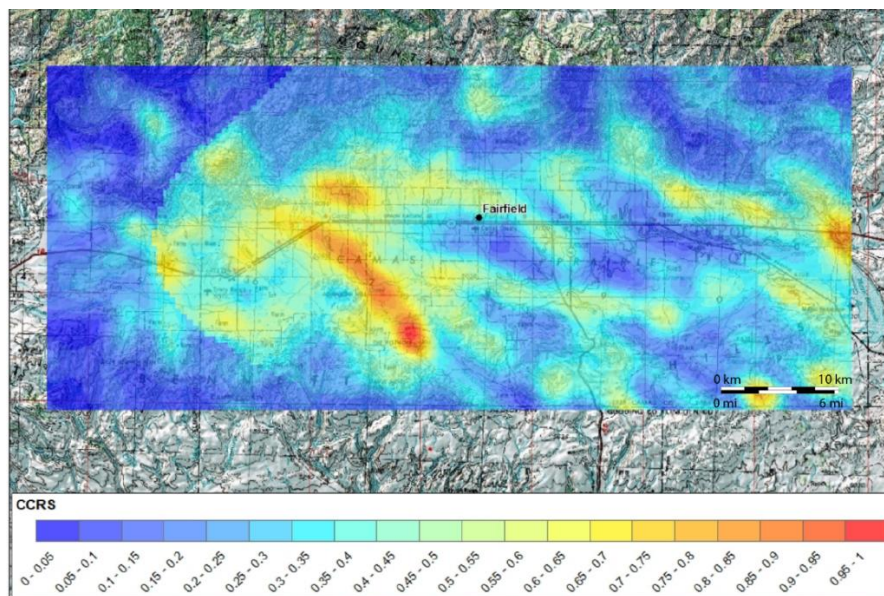
Figure 5. CCRS map of the Camas Prairie (Shervais et al., 2017). Areas depicted in red are more favorable for exhibiting a geothermal resource, while areas in blue express a low favorability. The area of highest favorability stretches along the Pothole fault network, trending NW-SE.

METHODS

To assess the geothermal potential of the Camas Prairie, the following data were collected and reviewed. Lithology of the cuttings and core was determined by in-field examination using rudimentary techniques. Mineralogy of the core was determined by X-ray diffractometry (XRD). Temperature logs were conducted throughout the extension of the borehole by attaching a HOBO device to the core barrel and lowering the apparatus down the hole. Geophysical data were collected by the USGS Research Drilling Geophysical unit with a wired sonde in much the same fashion as the HOBO device. Pressure data were collected on October 21 and 23, 2018 and November 4, 2019 by sealing the well and injecting fluids. Cations were analyzed in house via Inductively Coupled Mass Spectrometry (ICP-MS) under EPA Method 6020 and using acidified splits. Anions were analyzed by the Utah Water Research Laboratory (UWRL) via Ion Chromatography (IC) using unacidified water samples collected in August of 2019 when the USU Camas-1 well was flowing artesian. Deuterium (^{2}H) and oxygen-18 (^{18}O) isotopes were measured using Isotope Ratio Mass Spectrometry (IRMS). Reservoir temperatures were calculated using classic geothermometers such as the Giggenbach (1988) Na/K. The discharge rate was measured in July 2019 using the bucket and stopwatch method.

Rock Sampling

As mentioned above, drilling of the borehole was initially made using rotary techniques. Rock samples were collected during the initial drilling period of the USU Camas-1 well in the form of cuttings. Circulating fluids lifted rock cuttings to the surface. Cuttings were logged on site by sifting through the slurry and washing away circulating mud.

Rock core was retrieved at intermittent intervals below ~335 m (1,100 ft). Particularly fractured sections of core made progress difficult, necessitating extraction. Given the fractured nature of the core, some periods of coring were significantly shorter than others. The maximum footage that could possibly be gained during a single run was 3.05 m (10 ft). However, most runs did not reach that length, and on one occasion the footage gained was only 0.15 m (0.5 ft) before coring was suspended and the core retrieved.

Core was logged at the convenience of the drillers. Reported were percent recovery, lithology and mineralogy, condition of core (i.e., how cohesive the core was upon extraction from the core barrel), footage gained, current depth, date, time, and box and run number. Footage was recorded upon retrieval of the core, and the core was measured immediately after being deposited on the shuttle trough used to transport the core into the field station for review, logging, and boxing.

Occasionally the core barrel would get blocked by a piece of core from a particularly fractured section behind which water pressure would build until it was released all at once, ejecting the core sections with great force and scattering the pieces up to tens of meters. Projectiles of core were gathered and rearranged to the best of the geologists' abilities. However, the orientation of these sections remained ambiguous, and subsequently the core was marked with a question mark at these locations.

Mineralogy was determined directly by examining the core under hand lenses, applying dilute HCl acid to the surface of the core, and examining the core under a binocular microscope. Later, the assigned mineralogy was validated and refined in the lab using XRD.

Mineralized surfaces of the core and alteration facies were preferentially selected for XRD analysis. Samples were pulverized using a rock mill prior to being analyzed by the PW340/60 console X'Pert Pro X-Ray Diffraction System. An angle range of 2-75° was used to identify the minerals present. X'Pert HighScore software was used to match peaks automatically, while the rest of the peaks were matched manually.

Geophysical Logs

Several geophysical log runs coincided with the extension of the borehole via rotary methods, while only one geophysical log run was conducted after the hole was cored to its TD. During the geophysical log that followed coring, material sloughed off the walls of the borehole and effectively trapped the sonde. Retrieval efforts proved futile, so the sonde was abandoned. Fortunately, data were logged during the sonde's descent via the wired connection.

The variables measured during these log runs were gamma ray, resistivity, conductivity, spontaneous potential (SP), delta t and temperature. Gamma ray measures the natural gamma radiation emitted from materials surrounding the sonde. Potassium (K^+), thorium (Th^+), and uranium (U^+) cause spikes in gamma ray measurements. Lithologies with high K^+ contents, like rhyolite, have higher gamma ray readings than lithologies lacking in these radioactive constituents.

Resistivity, conductivity, and SP are electrical prospecting techniques. Resistivity logs measure the formation's resistance to the flow of an injected electric current. A porous medium with interconnectivity between pores and groundwater occupying those pores will report relatively low resistivity values. Clays will act to increase the formation's resistance to the flow of an electric current and thus cause high resistivity readings. Conductivity logs measure the

conductance of an induced current flow and are the inverse of resistivity logs. Spontaneous potential logs measure the static electrical potential between a grounded node at the surface and the sonde at depth, and requires the use of a conductive drilling fluid.

Delta t, also referred to as interval travel time or interval transit time, is the measure of time that it takes for a wave to travel a specific distance. The typical unit used for delta t is µsec/ft. One can use the consistent transit time of steel casing (57 µsec/ft) to distinguish between formation and casing. Sedimentary units typically fall in the range of 140 to 160 µsec/ft.

Temperature logs are somewhat self-explanatory but measure the temperature of the fluids in the borehole. This is a useful log in determining where geothermal fluids might be entering a well and where cold injection/drilling fluids may be entering the formation.

Temperature

Temperature logs were measured using a HOBO device that was programmed to measure at set intervals; in this case the interval was every ten seconds. On October 24, 2019, the device was programmed to record temperature in increments of ten seconds and to begin recording at a specified time. At every increment, the HOBO device measured and recorded a temperature. The HOBO device was attached to the wireline and placed into the hole five minutes after the specified time that the device was programmed to begin recording. The time at which the HOBO device entered the hole was recorded, and the rate at which it descended and ascended was kept constant at 2 ft/s. The device was left on the bottom of the hole for 10 minutes before beginning its ascent.

Once the temperature run was complete and the device was retrieved from the hole, the data were downloaded to a laptop computer and Microsoft Excel™ was used to convert the

column of time to depth, which was a simple calculation given the increment at which the HOBO device recorded temperatures and the steady rate at which it advanced down and back up the hole. Plots of separate temperature logs show similar temperature trends with respect to depth, which are discussed in detail in the Results.

Pressure Test

Two injection tests were conducted shortly after completion of the USU Camas-1 well to a depth of ~491.3 m (1,612 ft) to determine formation characteristics of the well. During both tests, a temperature and pressure tool was lowered and set in the hole at a depth of 373.4 m (1,225 ft). The first pressure test was performed on October 21, 2018. Due to failure on the part of the pressure and temperature tool to execute properly, as per manual setup, downhole pressure data was not recorded during the first test. The tool did, however, function properly for the second test on October 23, 2018, during which downhole pressure data was recorded. A leaky surface packer necessitated that the injection rates be kept low during the two tests at ~1.4 L/s (22 gpm) for the first and ~1.0 L/s (16 gpm) for the second.

The third and final injection test occurred on November 4, 2019 following the completion of the well to its TD of ~618 m (2,028.5 ft) and was done using a device assembled at the surface prior to the run. Once the battery pack was connected, the tool started recording, hence the lag between recording start time and entry of the hole at ~17 minutes. The data recorded were depth, time, line speed, temperature, and pressure. Since the device was placed in the 15-cm (6-in) inner diameter (ID) rod the results should, in theory, duplicate those of the previous year's test. However, due to "threading issues" involving an overlap between the 15-cm (6-in) ID rod and H-rod at a depth range between 323 m (1,060 ft) and 347 m (1,139 ft), the tool got hung up and required multiple sets of raising and lowering to get through this section. The device was

eventually lowered to a depth of ~373.4 m (1,225 ft) at an arbitrary rate at which point the well

was sealed. Injection then began and was held constant at a rate of 37 gpm (~2.3 L/s). The device

remained at a depth of ~373.4 m (1,225 ft) for 4 hours and 17 minutes until it was brought back

to the surface at a rate that fluctuated between 1 and 2 m/s.

Water Sampling and Analyses

Water samples were collected under artesian conditions during August of 2019, prior to

the subsequent coring of the well in the fall. Prior to sampling, the well was opened and purged

for >2 hours. To collect water samples, rubber tubing was placed inside the well flow port. This

hose was attached to a hollow metal coil surrounded by ice and a filtration device. Feeding the

sample through the coil effectively lowered the temperature of the scalding samples. One set of

duplicates was acidified using HCl while the other set was left unacidified. Water samples were

then transported to the USU campus directly for analysis.

Cations and stable isotopes were analyzed from USU Camas-1 well water samples via

ICP-MS and IRMS, while anions were analyzed via IC. The ICP-MS and IRMS runs were

conducted inhouse using the Utah State University Stable Isotope Laboratory's (USUSIL)

Thermo X Series 2 Quadropole ICP-MS and ThermoFisher Scientific Delta V Advantage IRMS

coupled with a Gasbench II Interface. Cations were analyzed using the ICP-MS device, while

stable isotopes of ^{18}O and ^{2}H were analyzed using the IRMS instrument. Both inhouse and

international standards were used to calibrate the data. Following the Nelson (2000) method that

accounts for drift in the samples of stable isotopes, a linear regression plot between the Vienna

standard mean ocean water (VSMOW) and Standard Light Antarctic Precipitation (SLAP) was

used. Water samples were sent to the Utah Water Research Lab (UWRL) to be analyzed by the

Dionex DX-500 ion chromatograph for anion concentrations.

Stable isotopes of ^{18}O and ^2H are reported in δ notation with units of per mil (‰), a ratio comparing the concentration of the heavy isotope in the water sample to a standard. Values of δ are calculated by collating the measured concentrations of the heavier isotope to the standard mean ocean water (SMOW), or another standard, via the following equation:

$$\delta = [\frac{Rsample - Rstandard}{Rstandard}] \times 1,000$$

R_{sample} can either be $^{18}O/^{16}O$ or $^2H/H$, and $R_{standard}$ is the ratio of the equivalent heavy and light isotopes for the SMOW. The $R_{standard}$ value used to calculate the δ values were $^{18}O = 3.9948 \times 10^{-3}$ and $^2H = 3.16 \times 10^{-4}$ (Mazor, 1990).

It was suspected that high concentrations of major anions in the water samples necessitated their dilution prior to being submitted to the UWRL. However, many of the constituents measured below their detection limits. Consequently, a set of undiluted samples was submitted as well.

A bicarbonate (HCO_3^-) concentration of ~213.6 mg/L was determined by performing a titration. By plugging the bicarbonate concentration into a cation-anion balance equation with the other ion concentrations, it is possible to assess the quality of the ion data. If the cation-anion balance falls within a range of ±5% of zero, then the ion data will be accepted (Figure 6).

Geothermometry

Reservoir temperatures were calculated using geothermometry. The assumptions for geothermometry calculations are outlined by Marini (2000) as: (1) geothermal fluids and relevant minerals reached equilibrium inside the geothermal reservoir, (2) no dissolved constituents precipitated out of solution once the geothermal fluids exited the reservoir, (3) no dissolution of
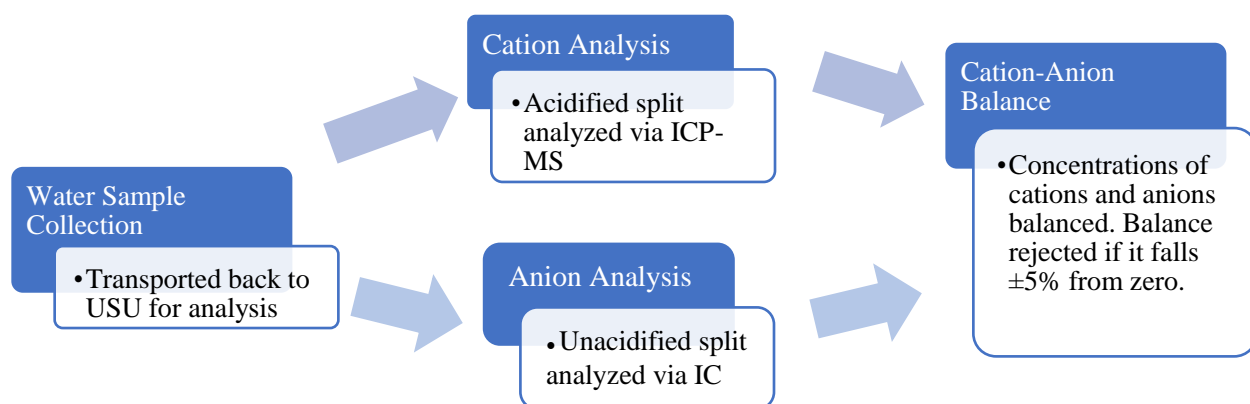
Figure 6. Flow chart showing the process of collecting ion concentration data.

rocks occurred outside of the system that would increase the concentrations of dissolved

constituents, (4) the pore-fluid pressure of the reservoir was held constant by the coexistence of

liquid and steam, and (5) mixing did not occur during the ascent of the geothermal fluids. These

assumptions allow geochemists to perform geothermometry on geothermal fluids sampled

outside of the equilibration reservoir. However, proving that these assumptions took place is

often difficult and is not fulfilled everywhere (Fournier et al., 1974; Ferguson et al., 2009).

As water migrates out of the geothermal reservoir and makes its way to the surface, it

cools on the way up. A cooling water sample could mean that some dissolved constituents

precipitate out of solution or in the case of calcite, become soluble. These effects are negligible

based on the assumptions above, as well as sampling protocols outlined in the Water Sampling

and Analysis section (samples were filtered at the surface and splits were acidified).

The geothermometry equations used to calculate reservoir temperature in this study are

the quartz and chalcedony (Fournier, 1977), two Na/K equations (Fournier, 1979; Giggenbach,

1988), Na-Ca-K (Fournier and Truesdell, 1973), Na-K-Ca-Mg (Fournier and Potter, 1979), and

the K^2/Mg (Giggenbach, 1988). These equations can be found in Table 1.

Table 1. Table containing the equations that were used to estimate reservoir temperature, the solute used, and the reference. (Units of concentration vary from equation to equation: equivalents for Fournier & Potter (1979), molality for part of the Fournier & Truesdell (1973), and ppm-mg/kg-mg/l for the rest.)

Solute	Equation	Paper
Quartz	$T(°C)=\dfrac{1309}{5.19-\log\,(SiO2)}-273.15$	Fournier, 1977
Chalcedony	$T(°C)=\dfrac{1032}{4.69-\log\,(SiO2)}-273.15$	Fournier, 1977
Na/K	$T(°C)=\dfrac{1217}{\log\left(\frac{Na}{K}\right)+1.483}-273.15$	Fournier, 1979
Na/K	$T(°C)= [1390/(1.75+\log(Na/K))]-273.15$	Giggenbach, 1988
Na-K-Ca	$T(°C)=\dfrac{1647}{\log\left(\frac{Na}{K}\right)+\beta\left[\log\left(\frac{\sqrt{Ca}}{Na}\right)+2.06\right]+2.47}-273.15$	Fournier & Truesdell, 1973
Na-K-Ca-Mg	$T(°C)=\dfrac{1647}{\log\left(\frac{Na}{K}\right)+\beta\left[\log\left(\frac{\sqrt{Ca}}{Na}\right)+2.06\right]+2.47}-273.15$ $-\Delta t_{Mg}$	Fournier & Potter, 1979
K^2/Mg	$T(°C)= [4410/(14.0-\log(K^2/Mg))]-273.15$	Giggenbach, 1988

Solubilities of solutes in the thermal fluid are dependent on temperature. The concentration of most dissolved constituents increases as temperature increases. When these dissolved constituents equilibrate in their geothermal reservoirs, calculations can be performed to determine a representative reservoir temperature, assuming the fluid did not re-equilibrate after leaving the reservoir. Factors that could cause re-equilibration of geothermal fluids are reactive wall rocks, low flow rate, a relatively long path of ascent, and kinetics of the reaction(s) taking place (Fournier, 1977). Calculations that produce lower temperature estimates for the reservoir than the greatest temperature recorded in the well, ~81°C, are adjusted according to potential re-equilibration influences.

Quartz is a relatively reliable geothermometer. The concentration of quartz is not affected by the loss of volatiles or by ion effects. Quartz also does not form complexes like other solutes. Generally, the abundance of reactants is sufficient for silica equilibration (Fournier, 1977). The

Fournier (1977) quartz calculation used to estimate reservoir temperature can be found in Table 1

with the rest of the equations. To calculate a reservoir temperature using quartz, one must select

and use the most appropriate of two solubility curves, the solubility curve corrected for

maximum steam loss and the no-loss-from-steam solubility curve. If boiling likely occurred prior

to sampling, one should use the maximum steam loss curve. If the water sample likely cooled by

conduction, one should use the no-loss-from-steam curve. In the case of the Camas Prairie water

samples, the solubility curve that does not take steam loss into account was selected. For lower

temperature systems, ≤75°C, the quartz equation has been modified to account for the SiO_2

iterations that dominate the fluid under these conditions, chalcedony being one of them

(Fournier, 1977).

Na/K ratio calculations are most reliable for waters that equilibrate at ≥200°C (Li et al.,

2020). Waters that equilibrate at temperatures colder than 100°C produce anomalously high

reservoir temperature estimates when using the Fournier (1979) Na/K ratio equation. When

dealing with colder waters, <100°C, it advisable to use the Na-K-Ca equations (Fournier and

Truesdell, 1973; Fournier, 1977). Calcium-bearing minerals, such as calcite, lining the wall rocks

of geothermal reservoirs may prevent proper equilibration of geothermal fluids and result in

waters that possess muted concentrations of Na^+ and K^+. For this reason, Fournier and Truesdell

(1973) created the Na-K-Ca equation. The value of β used in the Na-K-Ca and Na-K-Ca-Mg

equations will be 1/3 if $\log\sqrt{(Ca)}/Na + 2.06 < 0$. If $\log\sqrt{(Ca)}/Na + 2.06 > 0$, a value of 4/3 should

be used for β instead (Fournier and Truesdell, 1973). If the calculated reservoir temperature is

>100°C when using a value of 4/3 for β then a value of 1/3 should be used to recalculate the

reservoir temperature. Molality should be used for units of concentration.

For the magnesium correction conceived by Fournier and Potter (1979), one should first calculate the reservoir temperature using the Na-K-Ca equation discussed above (Fournier and Truesdell, 1973). If the calculated reservoir temperature is <70°C using the Na-K-Ca equation, a magnesium correction is not necessary. However, if the calculated temperature is >70°C, the next step will be to calculate R, using the equation: R = [Mg/(Mg + Ca + K)] x 100. The unit of cation concentration to be used is equivalents. A yielded R value >50 indicates a colder reservoir with temperatures matching those measured during sampling. If $5 < R < 50$ then Δt_{Mg}, the temperature in °C to be subtracted from the Na-K-Ca estimate, should be calculated as: $\Delta t_{Mg} =$ 10.66 - 4.7415R + 325.867$(\log R)^2$ - 1.0321 x $10^5(\log R)^2/T^2$ -1.9683 x $10^7(\log R)^2/T^2$ + 1.6053 x $10^7(\log R)^3/T^2$. In this equation, R represents the percent Mg/(Mg + Ca + K) and T is the Na-K-Ca temperature estimate in degrees Kelvin. If $0.5 < R < 5$ the following equation should be used instead: $\Delta t_{Mg} =$ -1.02995 + 59.97116(logR) + 145.049$(\log R)^2$ -36711.6$(\log R)^2/T$ – 1.67516 x 10^7 (logR/T). Finally, if R < 0.5 no correction is applied. Likewise, if the calculated Δt_{Mg} is negative, no correction is applied.

The Na-K ratio equation (Giggenbach, 1988) is reliable when the pH of the system is close to neutral. The reservoir temperature calculated using this equation should, therefore, be a representative one for the Camas Prairie.

RESULTS

Formation Characteristics

Drilling

The USGS Research Drilling unit performed the drilling. The USGS drilling team used a multimethod top head TH60DH rig to drill via rotary techniques for the first ~491.3 m (1,612 ft) bgs of hole, and cored the remaining section of hole to its maximum depth of ~618.3 m (2,028.5 ft) bgs using a Christensen CS 1000 P6L rig. A 9 7/8-in (25.1-cm) pilot hole was first drilled from 0-12.8 m (0-42 ft) bgs and then reamed with an 18-in (45.7-cm) rotary bit (Figure 7). A 12 3/4-in (32.4-cm) outside diameter (OD) conductor casing was then set and cemented. From 12.8 to 347.5 m (42-1,140 ft) bgs a 7 7/8-in (20-cm) hole was drilled and then reamed to 12 in (30.5 cm) down to 323 m (1,060 ft) bgs. The hole was then further reamed with a 9 7/8-in (25.1-cm) tricone bit to 346.9 m (1,138 ft) bgs and set with 6 5/8-in (17.1-cm) OD 0.25-in (0.6-cm) wall steel casing, which was cemented into the annular space. The hole was then drilled to 491.3 m (1,612 ft) bgs using a 5 5/8-in (14.3-cm) tricone bit. H-rod was then installed 3 ft (0.9) into new rock as temporary casing and subsequently twisted off at a depth of 490.4 m (1,609 ft) bgs. Finally, the hole was cored with NQ-rods to TD at ~618.3 m (2,028.5 ft). Plans to cement the full borehole interval were aborted due to complications with the geophysics sonde and H-rod.

Cuttings

Various pieces of evidence supporting the presence of a permeable and/or productive zone somewhere between 344.4 and 359.7 m (1,130 and 1,180 ft) bgs, to be discussed later in detail, are why this interval of cuttings was selected for review. The indicators of geothermal fluid flow sought after during review were mineralization and alteration facies. Upon first review

Drilled 9 7/8" pilot hole, then
reamed with 18" bit to 42'

Reamed to 12" (42-1060')

6 5/8" OD 0.25" wall A53B steel casing

5 5/8" borehole

0-42' - 18" borehole
12.75" OD conductor
cement annular

42-1060'
Rotary drill with 7-7/8" bit
from 42' to 1140', then reamed
with 12" bit to 1060', switched
to 9-7/8' tricone bit to ream
down to 1138'.
Set 6-5/8" steel casing to
1138' and cemented
annular space.

Used Halliburton cementing
shoe and pumped down
cement with wiper, locked it
in and held pressure.
Upper few feet of annular
space finished off by pumping
cement down with 1" grout
hose. 5-5/8" PDC used to drill
out rubber wiper and
cementing shoe. Drilled to
1144' and well made a lot of
water, so tripped in tremie to
1140' and cemented off the
bottom to 965'

Drilled to 1612'
with 5-5/8" rotary bit.

H-rod set as temporary
casing 3' into new rock
with casing shoe.

H-rod stuck in hole;
twisted off at 1609'

Cored with NQ-rod
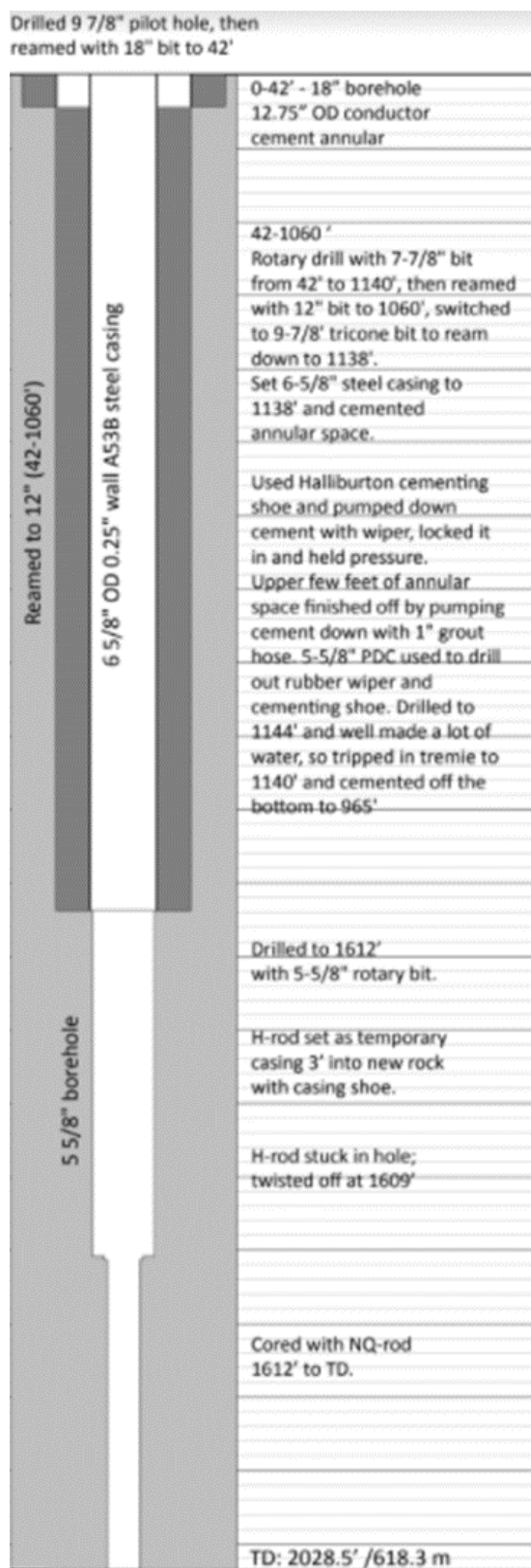1612' to TD.

TD: 2028.5' /618.3 m

Figure 7. Schematic of borehole.

of the cuttings in this interval, it would seem to show two instances of mineralization and alteration (Figure 8) between 344.4-347.5 m (1,130-1,140 ft), and between 353.6-359.7 m (1,160-1,180 ft). However, upon further review the whitish-grey material found in Figure 8E and 8F between the depths of 353.6 and 359.7 m (1,160 and 1,180 ft) bgs is not mineralization but siltstone. The only instance of mineralization in this section therefore occurred between the depths of 344.4 m and 347.5 m (1,130 and 1,140 ft) bgs (Figure 8A). Driller reports state that a productive zone was encountered at a depth of ~346.9 m (1,138 ft) bgs on September 27, 2018. On this day only 12.2 m (40 ft) was gained, compared to a gain of 48.8 m (160 ft) the day prior, suggesting that the rock is harder in this section than above it. The cuttings of this section are of two compositions: an altered chlorite-bearing greenish volcanic unit, possibly andesite, with abundant calcite and an orangish-brown silicified aphanitic unit. Since no chips contain both types of rock, the two units are apparently alternating and distinct.

XRD

Relevant XRD diffractograms are presented in Figure 9; all other diffractograms can be found in Appendix A. Altered facies and mineralized surfaces were preferentially sampled and analyzed. Matches were quantified using score (0-100) and scale factor (0-1.000). The mineralized surface at ~542.8 m (1,781 ft) bgs (Figure 9 A) contains quartz (score: 52, scale factor: 0.833) and albite (49, 0.307). Muscovite (25, 0.159), likely in the form of illite, was also selected as a match. Zeolite (23, 0.182) is a likely component as well since it matches several of the peaks but was not identified by the software as an outright match. However, gobbinsite (18, 0.090), a hydrothermal alteration mineral, is another likely candidate. The green chunk of core extracted from an approximate depth of ~504.4 m (1,655 ft) bgs (Figure 9 B) contains quartz (54, 0.529), muscovite/illite (25, 0.503), epidote (28, 0.045), and jacobsite (37, 0.043), a manganese

Figure 8. Cuttings retrieved from six consecutive 3.05-m (10-ft) intervals in the borehole A. 344.4–347.5 m (1,130-1,140 ft) bgs. B. 347.5-350.5 m (1,140-1,150 ft) bgs. C. 347.5–353.6 m (1,150-1,160 ft) bgs. D. 347.5–353.6 m (1,150-1,160 ft) bgs. E. 353.6–356.6 m (1,160-1,170 ft) bgs. F. 356.6–359.7 m (1,170-1,180 ft) bgs.
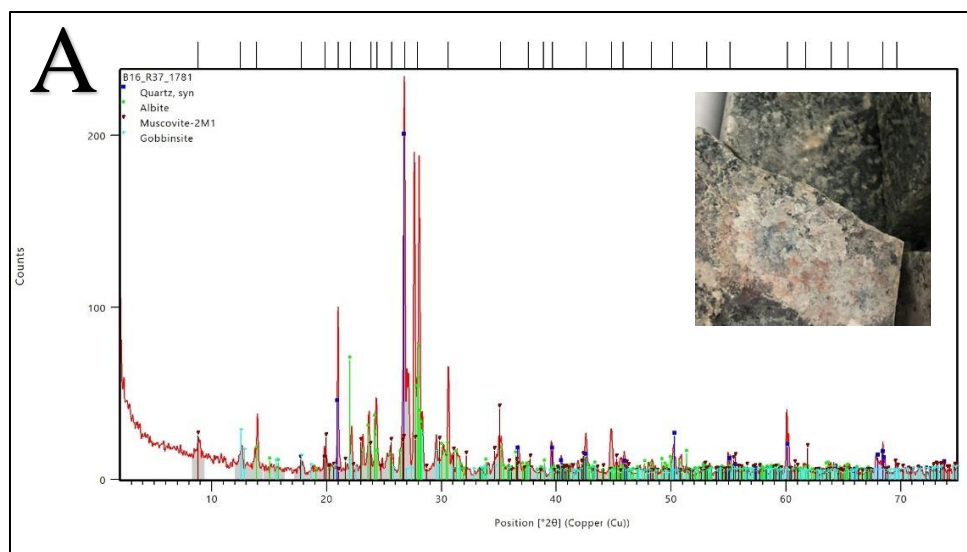
Figure 9. XRD results of four core samples. Mineralized surfaces and altered facies were preferentially sampled and analyzed. Image of each sample located in the top right-hand corner of its respective graph. A. Diffractogram of sample B16-R37-1781, a mineralized fracture of granitic rock.
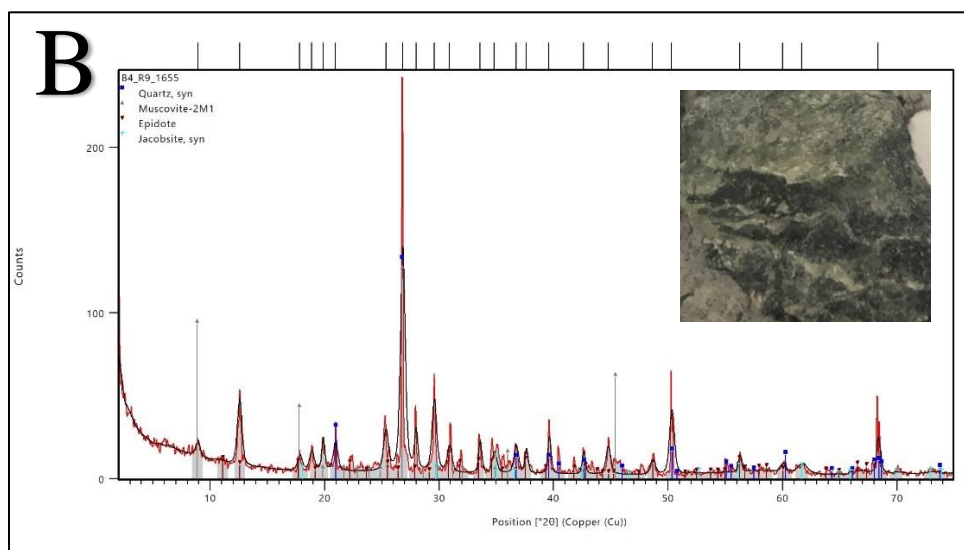
B. Diffractogram of sample B4-R9-1655, a green piece of core sampled from a section of granite.

oxide that would explain the darker colorization of the clast. Figure 9 C shows the diffractogram of a section of core identified as rhyolitic vitrophyre from a depth of ~498.3 m (1,635 ft) bgs. This unit was previously referred to as dacite, for its dark and thus seemingly mafic appearance,

but following a mineralogical analysis, it was discovered to contain more quartz (49, 0.937) than

was previously thought; hence the amendment in reference. This sample also contains albite (38,

0.600), clinochlore (33, 0.200), the dominant phase of chlorite, and anorthoclase (25, 0.179). The

final diffractogram (Figure 9 D) represents the fractured granite from ~517 m (1,696 ft) bgs.

Quartz (59, 0.335), albite (37, 0.262), and microcline (25, 0.212) were matched as its
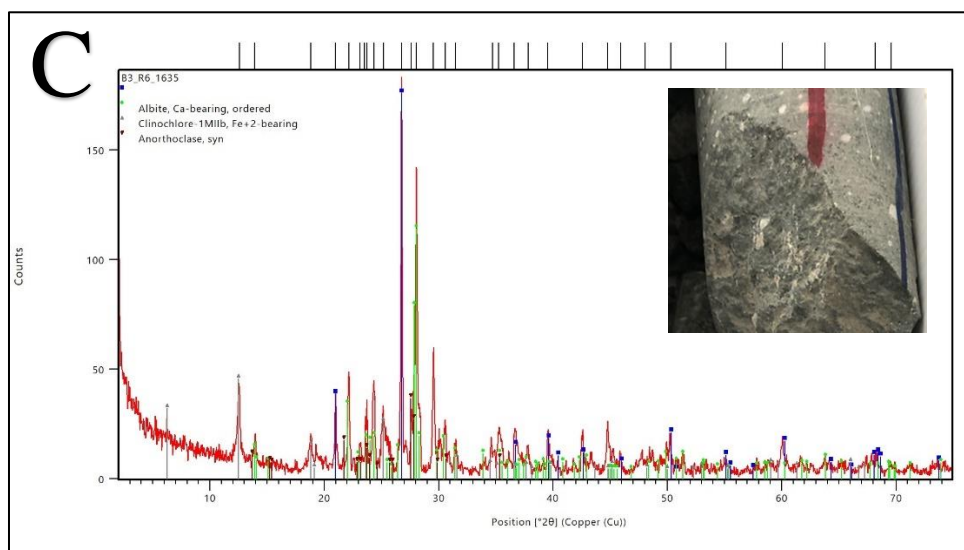
C. Diffractogram of sample B3-R6-1635, rhyolitic vitrophyre containing white phenocrysts
~3mm in diameter and 45° fractures ~3mm wide and calcite mineralization fill.
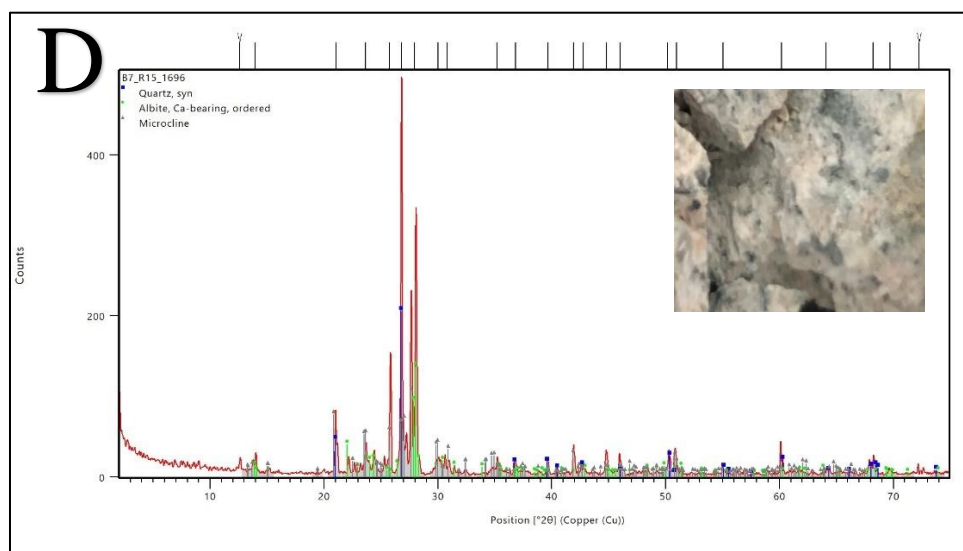
D. Diffractogram of sample B7-R15-1696, fractured granite.

constituents. Other diffractograms presented in Appendix A further support the presence of zeolites, hydrothermal alteration, and clays in the cored section of USU Camas-1.

<u>Lithologic and Geophysical Logs</u>

The lithologic log (Figure 10) shows that at the USU Camas-1 wellsite valley fill sediment composes the upper ~314 m (1,030 ft) of the borehole. Sediment in this upper section ranges in grain size from pebbly sand to clay. Soil and a silty clay loess compose the uppermost ~2.75 m (9 ft) of the subsurface. Granitic rock of the Idaho batholith, andesite, and rhyolite of various compositions and appearances likely belonging to the Idavada series underlie the sediments. Clay gouges were also found throughout the cored section of the hole but were too thin to be shown in Figure 10. Clay forms through hydrothermal alteration. As stated previously, the presence of a clay layer is key for any productive geothermal system to act as a seal.

Geophysical data were filtered to exclude spurious values. The excluded data include points that suddenly increased by one or more orders of magnitude, or dropped lower than the data above or below it for no apparent reason. A recurring value of -999.3 occurred across the different logs at overlapping sections of the borehole. This is a default value that acts as a placeholder for sections of borehole where no data is collected. The frequency at which geophysical data were collected above a depth of 346.9 m (1,138 ft) was one data point per 3.05 cm (0.1 ft). Between the depths of 346.9-373.5 m (1,138-1,225.4 ft), three data points of resistivity and SP were measured at every 3.05 cm (0.1 ft). Below a depth of 373.5 m (1,225.4 ft), six data points were collected for every 3.05 cm (0.1 ft). To solve this data frequency issue, the average value was calculated for each depth to produce a single data point for every 3.05 cm (0.1 ft).
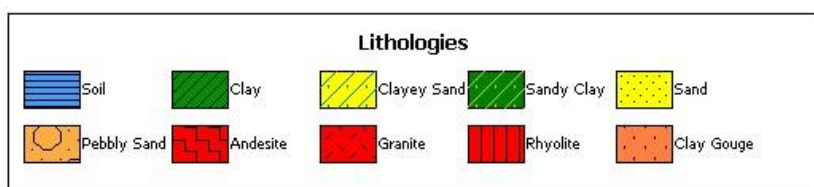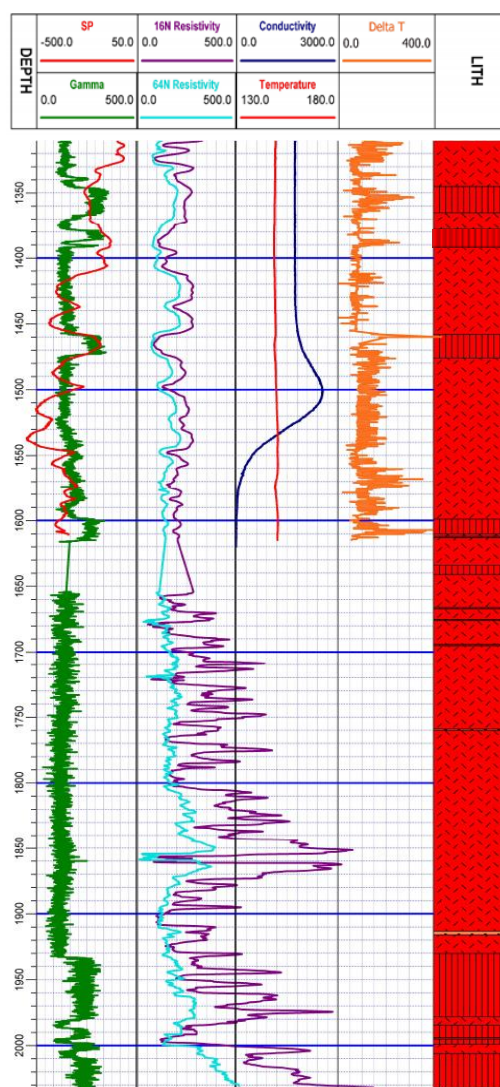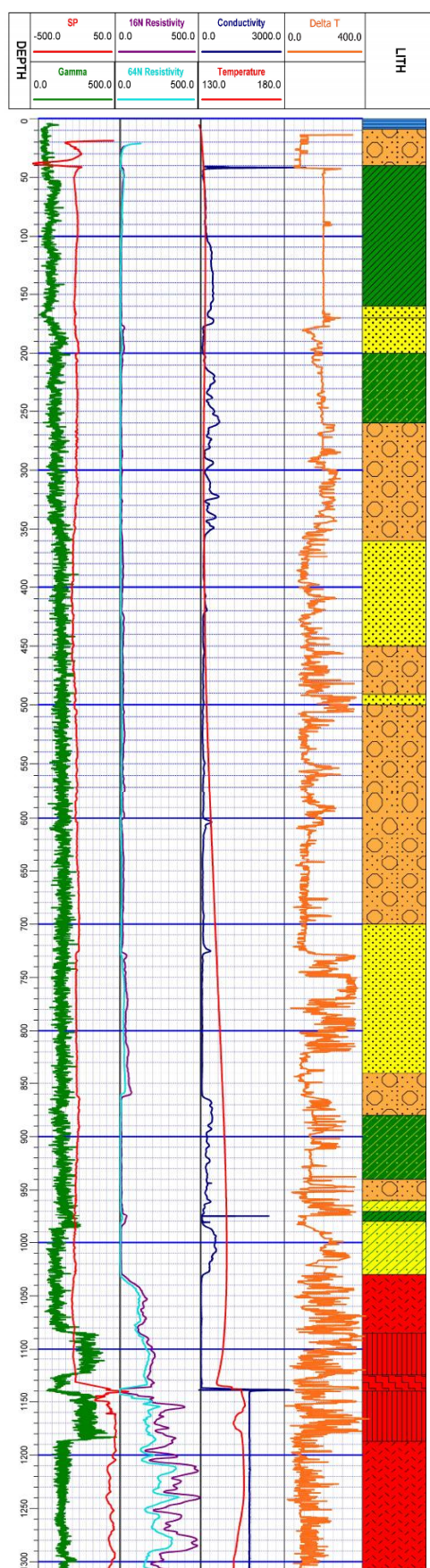
Figure 10. Geophysical logs of SP, resistivity, conductivity, gamma ray, and delta t plotted alongside a temperature log and lithologic log by depth for the USU Camas-1 well. SP is reported in mV, gamma ray is reported in API-GR, resistivity is reported in ohm-m, conductivity is reported in mmho/m, and delta t is reported in μsec/ft. A gap in the data between the second and third suites can be observed between the depths of 492.3 and 504.4 m (1,615 and 1,655 ft)

The first and uppermost suite of geophysical data was collected prior to casing in 2018 between depths of 12.8-347.5 m (42-1,140 ft). The middle section of hole was logged from 347.5-491.3 m (1,140-1,612 ft), and the final suite of geophysical logs was run from 492.3 m (1,615 ft) to the well's TD of ~618.3 m (2,028.5 ft) bgs. A gap of ~12.2 m (40 ft) exists between the second and third log suites. These runs were conducted by the USGS. Not all logs run for the first two suites were run for the final suite. Delta t, conductivity, and SP data were not collected during this run. It was during the final run that the sonde was lost due to a collapse in the hole. Had a sonde with a wired connection not been used for the final set of geophysical logs, data may not have been collected during the device's descent, and thus no data would be available for the lower section of the borehole.

Spikes in Camas Prairie delta t and gamma ray logs (Figure 10) correlate with sections of the core that are composed of rhyolite, an aphanitic rock of felsic composition that has a high potassium content. Elevated gamma ray readings are likely a reaction to higher contents of potassium feldspar in the rhyolite. Due to this correlation between spikes in gamma ray and the presence of rocks with high potassium content, it can be concluded that the sonde was functioning properly for gamma ray logs.

Since resistivity is an inverse measurement of conductivity and SP, it is expected to move opposed to the two logs. If resistivity rises and falls with conductivity or SP, the logs will need to be rejected. If the two logs move against one another, they will be accepted. The opposition is not perfect between the resistivity and conductivity. However, the SP log runs are opposed to the resistance logs well enough for the data to be accepted (Figure 10). One can readily observe the increase in resistivity that occurs at the interface between the relatively more permeable sediment overfill and the underlying felsic igneous rocks at 344.4 m (1,130 ft).

When the SP log spikes, the long and short resistivity logs (64 and 16 respectively) experience troughs. During the 259-317 m (850-1,040 ft) interval, the conductivity log also seems to run opposed to the resistivity logs. However, below a depth of ~347.5 m (1,140 ft) the conductivity log hovers around ~2,000 mmho/m then gradually ascends to a peak of ~2,600 mmho/m before descending to a point close to 0 at ~488 m (1,600 ft). Meanwhile, the resistance and SP logs experience many peaks and troughs over this interval.

At a depth of 347.5 m (1,140 ft) all electrical geophysical logs (SP, resistivity, and conductivity) experience either a peak or trough in the data (Figure 10). Both the long and short resistivity logs drop from ~175 ohm-m to nearly 0 ohm-m, while SP spikes to >50 mV. This is likely due to the presence of a permeable and productive zone, as suggested by rising temperatures measured at this depth. Directly below this spike in temperature, the temperature experiences a trough centered at 356.6 m (1,170 ft). This zone is also permeable but likely accepting cold water during drilling rather than supplying the well with hotter geothermal fluids. This phenomenon was first observed and hypothesized by Garg and Goranson (2018) during injection.

The lowest section of resistivity data between the depths of 504.4 m to TD at 618.3 m (1,655-2,028.5 ft) bgs has fluctuations with a much greater amplitude than the fluctuations of the resistivity data collected from previous runs (Figure 10). This is likely due to a faulty calibration at the surface prior to the final run. However, the gamma ray readings for this section continue the trend of responding to the high content of potassium feldspar in the rhyolite with a similar amplitude as above, and therefore the calibration is likely correct for gamma ray.

Temperature Survey and Pressure Tests

The temperature survey presented in Figure 11 was run on October 24, 2019, a day that did not coincide with drilling. The temperature profile shows two geothermal gradients that occupy the upper and lower sections of the well. The upper gradient occupies the first ~354 m (1,160 ft) of the hole. The descendant limb recorded a temperature of 12.9°C at a depth of 0 m, while the ascendant limb recorded a temperature of 25.8°C at zero. Taking the average of the two measurements produces a temperature of 19.4°C.

The maximum temperature of 80.3°C (ascendant; 79.5°C descendant) was reached within the range of the hypothesized permeable zone at a depth of ~354 m (1,160 ft). Subsequently, this depth and its average temperature [79.9°C at 354 m] was used along with the average
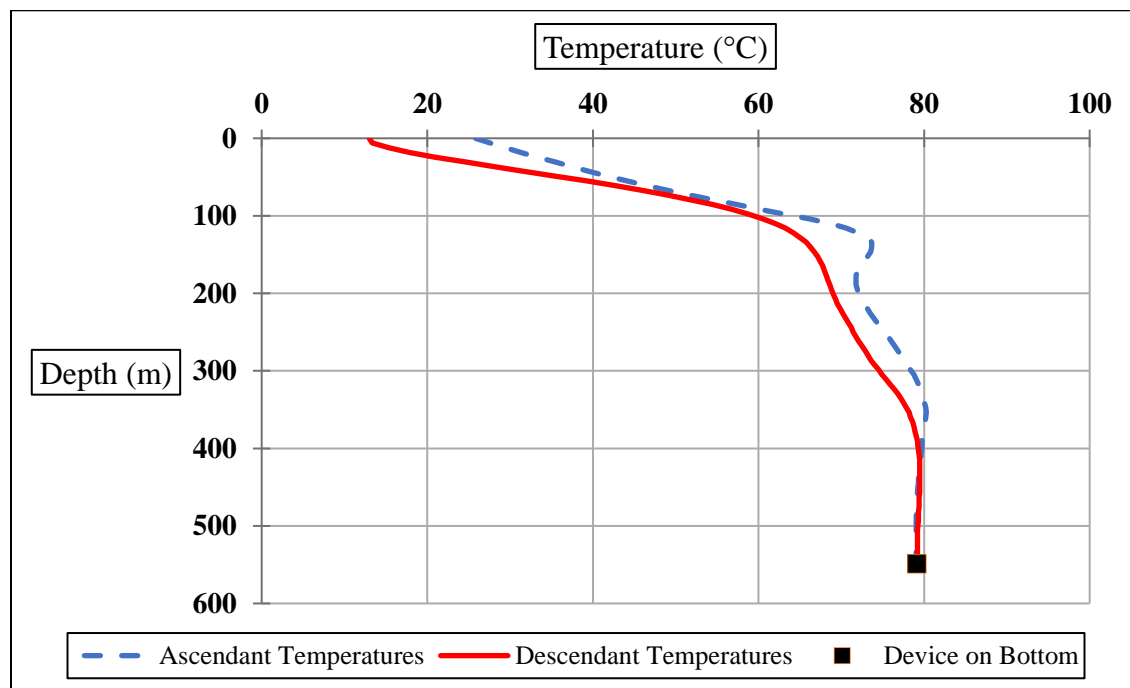

Figure 11. Plot of temperature survey conducted on October 24, 2019. The solid red line represents temperatures recorded during the HOBO device's descent down the borehole, while the dotted blue line represents temperatures recorded during its ascent. The black square represents the ten-minute period during which the HOBO device was left on bottom of the hole.

temperature mentioned above [19.4°C at 0 m] to produce the upper gradient of 169°C/km. Below

354 m the temperature remains relatively constant, making the lower-most gradient effectively

0°C/km. The shallower peak of the ascendant limb centered at ~134 m (440 ft) should be

discounted because the water/fluid column had been disturbed by the HOBO device, which

brought warmer, deeper water up from below ahead of it. Discrepancies between the descendant

and ascendant temperatures in Figure 11 are explained by this phenomenon, but could also be

due to equilibration of the probe.

On October 23, 2018, an injection test was begun under shut-in conditions on the USU

Camas-1 well. Depth, pressure, and temperature data were collected throughout the test. The

temperature run that followed the injection of cold water by 14 hours indicated a permeable zone

at ~357.5 m (1,173 ft) (Figure 12). It is at this depth that the data experiences a sudden drop from

~71°C to ~55°C. The temperature run that was conducted 59 days after injection exhibits the

same fluctuations at similar depths but with less amplitude (Garg and Goranson, 2018). The

maximum recorded temperature increased from 77.2°C at the bottom of the hole to 81.2°C at

~342 m (1,122 ft) (Figure 12).

The pressure survey shows a steady linear relationship between depth and pressure

(Figure 13). From the surface to a depth of ~490 m (1,607.5 ft) bgs, the pressure gradually

increases from 1 to ~47.4 bars. This is within the range proposed by Arnórsson et al. (1983) to

not influence equilibration of geothermal fluids. Extrapolating based on this pressure gradient

would place the depth at which pressure begins to influence solubility of geothermometers (200

bars) at >2,000 m.

The anomalous decrease in pressure at a stagnant depth of ~373.4 m (1,225 ft) with

continued injection makes the data between the rising limb and drop-off of the pressure test

unreliable for analysis (Figure 14 A); hence, the falling limb was used to estimate the

transmissivity of the permeable section (Figure 14 B). Two different methods of analysis by

Garg and Goranson (2018) on the falling limb of the pressure test produced transmissivity values

of 0.1 and 0.4 cm²/s (9 and 36 ft^2/d) for the hypothesized permeable zone.
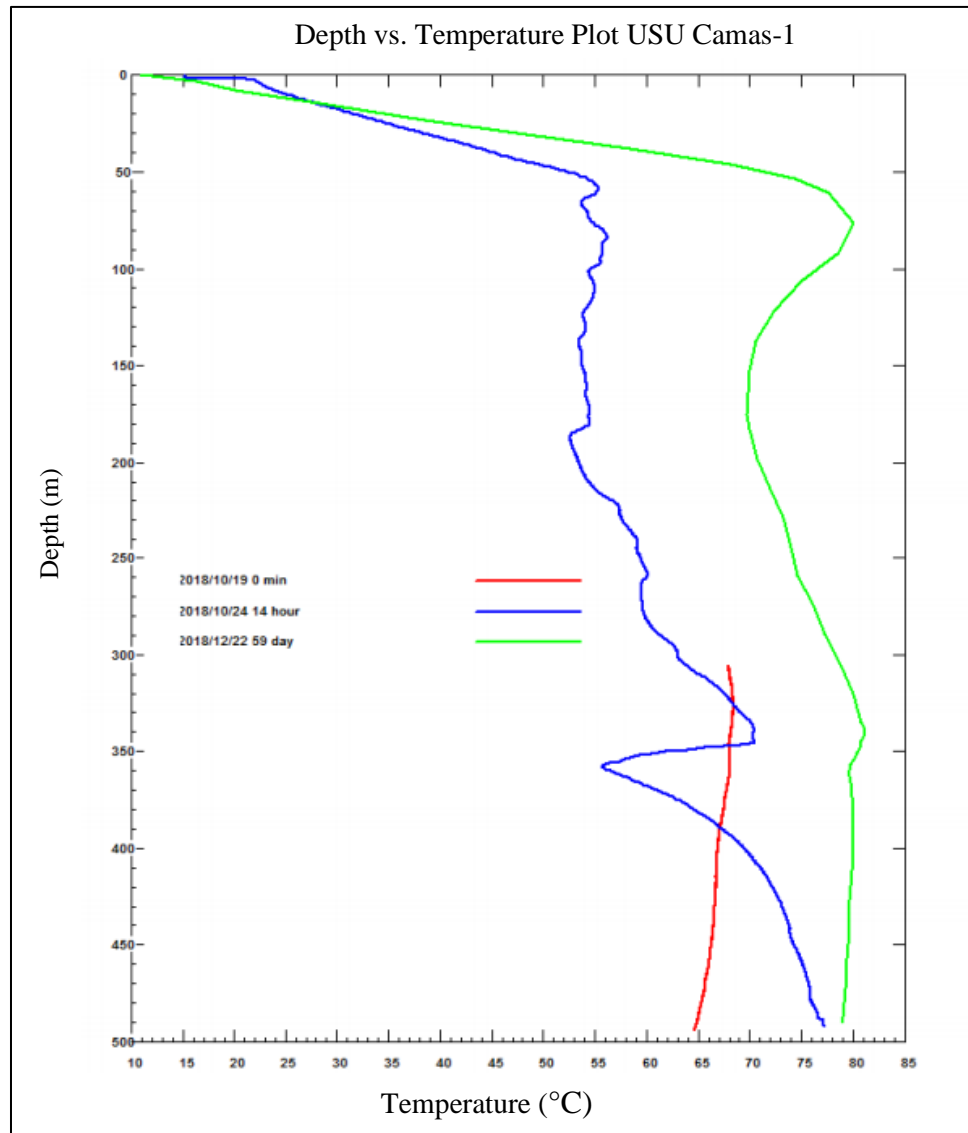
Figure 12. Temperature versus depth plots conducted under shut-in conditions following the injection of cold water into the USU Camas-1 well. The red line represents the brief and partial temperature data recorded at the start of the injection. The blue line represents the temperature run that occurred at 14 hours following injection, and the green line delineates the temperature run that commenced 59 days after injection, (adapted from Garg and Goranson, 2018).
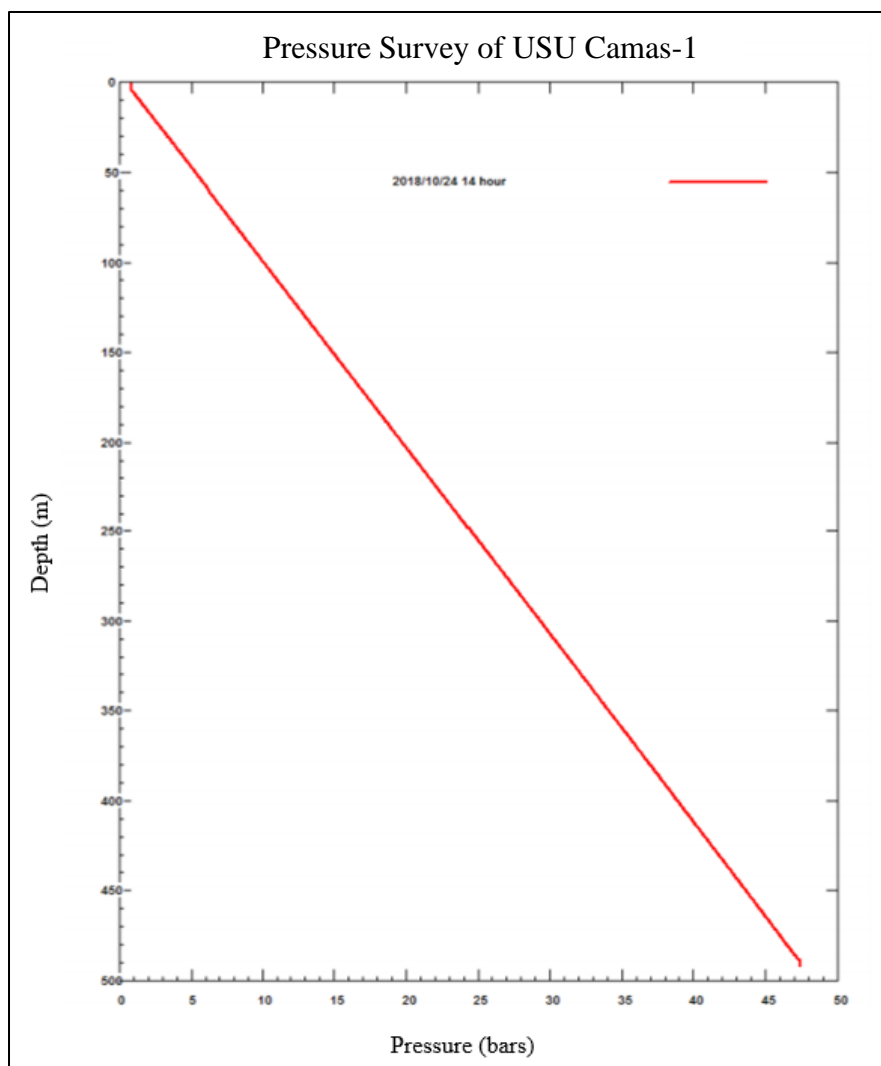
Figure 13. Pressure survey of USU Camas-1 well on October 24, 2018, (adapted from Garg and Goranson, 2018).

Hydrochemical Properties

<u>Major Ions</u>

The concentrations of ions measured in USU Camas-1 in August of 2019 are found in

Table 2 along with the concentrations measured by Freeman (2013) for the three Project Hotspot

wells. Abbreviations of the waters sampled by Freeman use two letters to represent the sampling

location, KA for Kimama, KB for Kimberly, and MH for Mountain Home, and subsequent

numbers to represent the depth at which the samples were collected. For the Kimberly samples,
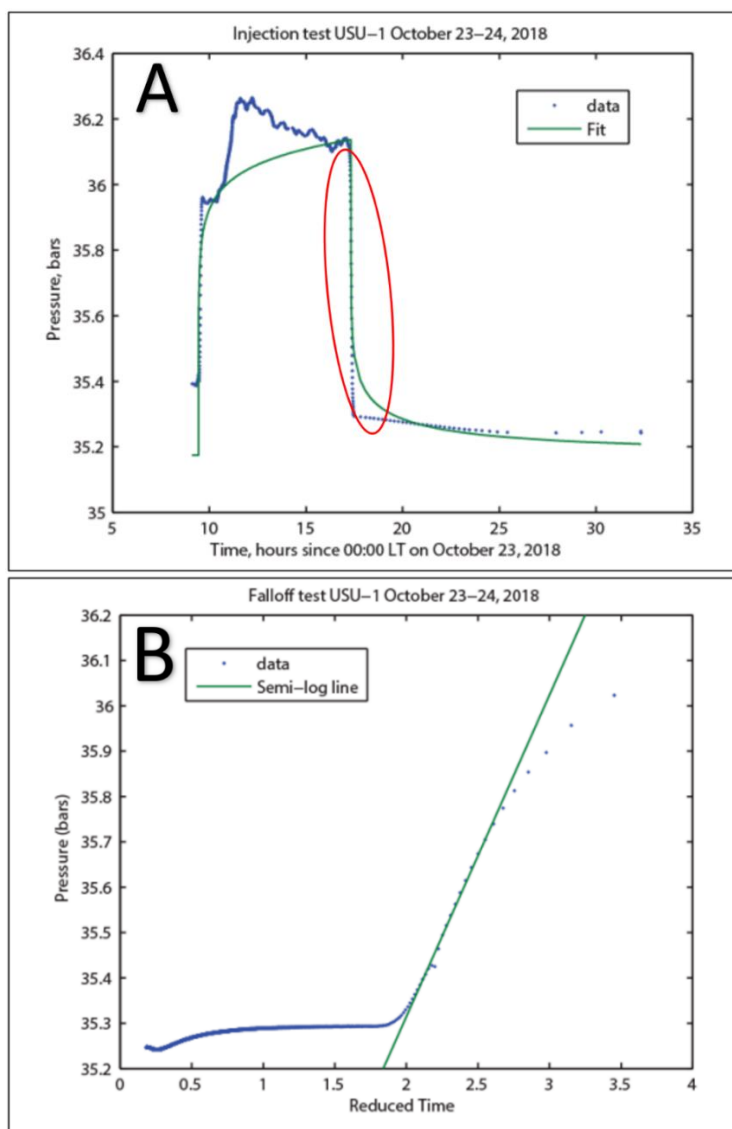
Figure 14. A. Pressure test associated with the injection test from October 23-24, 2018 and its mathematical fit, (falling limb circled in red). USU-1 refers to USU Camas-1. B. Horner plot of the falling limb, (adapted from Garg and Goranson, 2018).

the number correlates to hundreds of feet. For instance, KB-38 was sampled at a depth of ~3,800

ft (1,160 m) bgs. For the Mountain Home abbreviation, the number 5,726 is the actual depth in

feet at which the sample was collected (1,745.3 m). KA-1 was sampled from the Kimama well at

a depth of ~3,510 ft (1,070 m). Since the USU Camas-1 well was flowing artesian at the time of

its sampling, a depth distinction was not made for its abbreviation. The concentrations of less

common ions are presented in Appendix B.

Table 2. Chemical analyses of USU Camas-1 and Project Hotspot samples (all units in mg/L unless otherwise noted). The full suite of ion concentrations can be found in Appendix B.

Sample	T (°C)	EC (iS/cm)	pH (units)	Alkalinity (mg/L as CaCO$_3$)	Ca	Mg	Na	K	Cl	SO$_4$	SiO$_2$
USU Camas-1	71.9	925	8.76	164	2.29	0.17	97.5	2.53	11.7	13.5	81.2
KA-1	28.8	1,060	8.17	120	21.1	3.21	284	10.3	315	306	158
KB-38	23.3	2,970	7.60	1,100	24.7	10.1	562	17.9	204	7.29	94.5
KB-52	15.6	1,765	7.72	950	15.4	5.43	363	9.38	128	14.1	71.6
KB-63	17.7	2,568	7.83	850	23.8	9.33	541	13.2	189	13.8	76.7
MH-5,726	31.3	870	9.59	100	8.71	0.16	288	9.02	74.8	477	196

The concentrations of the major ions in the USU Camas-1 water may be due to the compositional differences between the rocks at each location. The subsurface of the Camas Prairie is comprised primarily of felsic igneous rocks rich in quartz and feldspars, while Mountain Home and Kimama are mostly basalts. The subsurface at Kimberly, which possesses a similar water chemistry to that of USU Camas-1, is composed mostly of rhyolite. Thus, the reason why the Kimberly well has higher concentrations of the major ions is due to differences in geothermal fluid residence time and not a difference in rock composition.

In high-temperature geothermal fluids, magnesium is present at extremely low concentrations, 10-100 ppb at 250-300°C (Mahon, 1965; Ellis, 1970). According to Ellis (1971), chlorite controls the concentration of magnesium. When encountering relatively high concentrations of magnesium, one must be wary of surface dilution or expect similar temperatures at depth as there are at the surface. Given the relatively low concentrations of magnesium in the USU Camas-1 water sample, this does not seem to be an issue.

Field measurements of water chemistry were made once in October 2018 and later in August 2019 at the time of water sample collection by Patrick Dobson and Hari Neupane. Not all

parameters measured in 2019 were measured in 2018 (Table 3). Since the USU Camas-1 well experienced flow to the surface in August but not in October, a discharge rate is available for the former (~0.7 L/s) but not for the latter. The bucket and stopwatch method was used to gather this measurement. The pH of the water at the time of sampling was 8.76. During drilling, the well water pH was 9.38. This is close to the pH of Freeman's (2013) Mountain Home sample (9.59). Freeman's (2013) other samples ranged in pH from 7.60-8.17. Electrical conductivity (EC) in the USU Camas-1 well was measured at 925 μS/cm. This is greater than the EC reading of Mountain Home (870 μS) and less than the Kimama and three Kimberly readings (1,060-2,970 μS). The USU Camas-1 well water had a dissolved oxygen measurement of 0.6 mg/L, an oxidation reduction potential measurement of -57.8 mV, and alkalinity measurements of 164 and 222 (mg/L as CaCO3) in August 2019 and October 2018, respectively.

Table 3. Field measurements of water chemistry in August 2019 at the time of water sample collection compared to those measured in October of 2018.

Sample	Temperature (°C)	pH (units)	DO (mg/L)	ORP (mV)	Conductivity (μS/cm)	Alkalinity (mg/L as CaCO$_3$)	Q (L/s)
Aug. 2019	71.9	8.76	0.6	-57.8	925	164	0.7
Oct. 2018	67.8	9.38	NA	NA	NA	222	NA

To characterize the USU Camas-1 water sample, major ion concentrations were plotted on a pair of trilinear diagrams (Figures 15 and 16). Using a trilinear diagram, it is possible to characterize a natural water based on the concentrations of the seven major ions: calcium, magnesium, potassium, sodium, bicarbonate, sulfate, and chloride. This type of trilinear diagram is known as a Piper (1944) plot.

The USU Camas-1 water sample belongs to the sodium-bicarbonate hydrochemical facies as identified by the Piper (1944) plot. The ionic composition of other waters sampled on the Camas Prairie by Mattson et al. (2016) also resemble that of the USU Camas-1 sample (Figure

15). The two samples collected at Elk Creek and the Barron W1 well contain significantly more

sulfate than the other Camas Prairie samples. However, most of the samples from the Mattson et

al. (2016) study group together in the sodium-bicarbonate hydrochemical facies.

The USU Camas-1 and all Project Hotspot water samples are rich in sodium (Figure 16).

Most samples plot together in the sodium-bicarbonate hydrochemical facies. However, Kimama

is dominated by sulfate and chloride, while Mountain Home is dominated by sulfate. In the USU
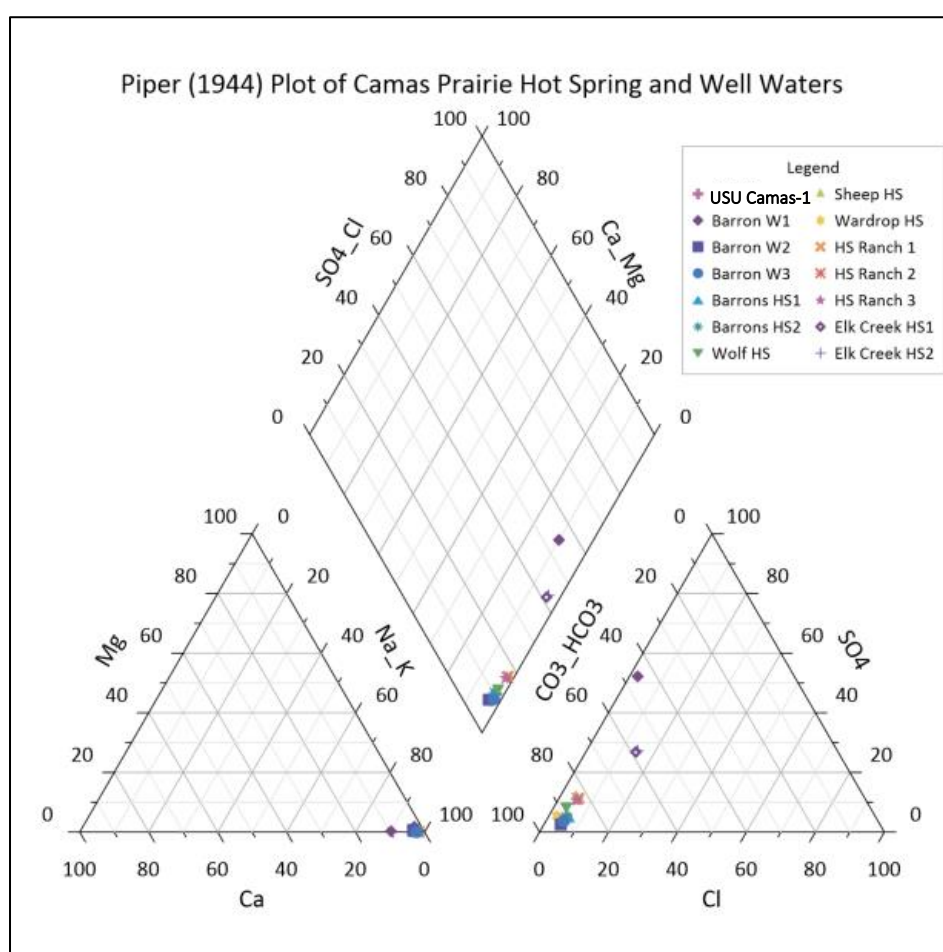

Figure 15. Piper (1944) diagram comparing major ion concentrations of the USU Camas-1 water
sample with other Camas Prairie water samples from Mattson et al. (2016).

Camas-1 water sample, and those from the Freeman (2013) study, the concentration of sodium is

far greater than that of potassium (Table 2). The concentration of magnesium in the USU Camas-

1 sample is 0.17 ppm and is on par with the 0.16 ppm magnesium concentration of the Mountain

Home sample (Table 2). These two samples boast the lowest concentrations of magnesium out of

the seven. It is well documented in the literature that high temperature systems (>175°C) have

low magnesium contents (White, 1968; Ellis, 1971; Arnórsson, 1978).
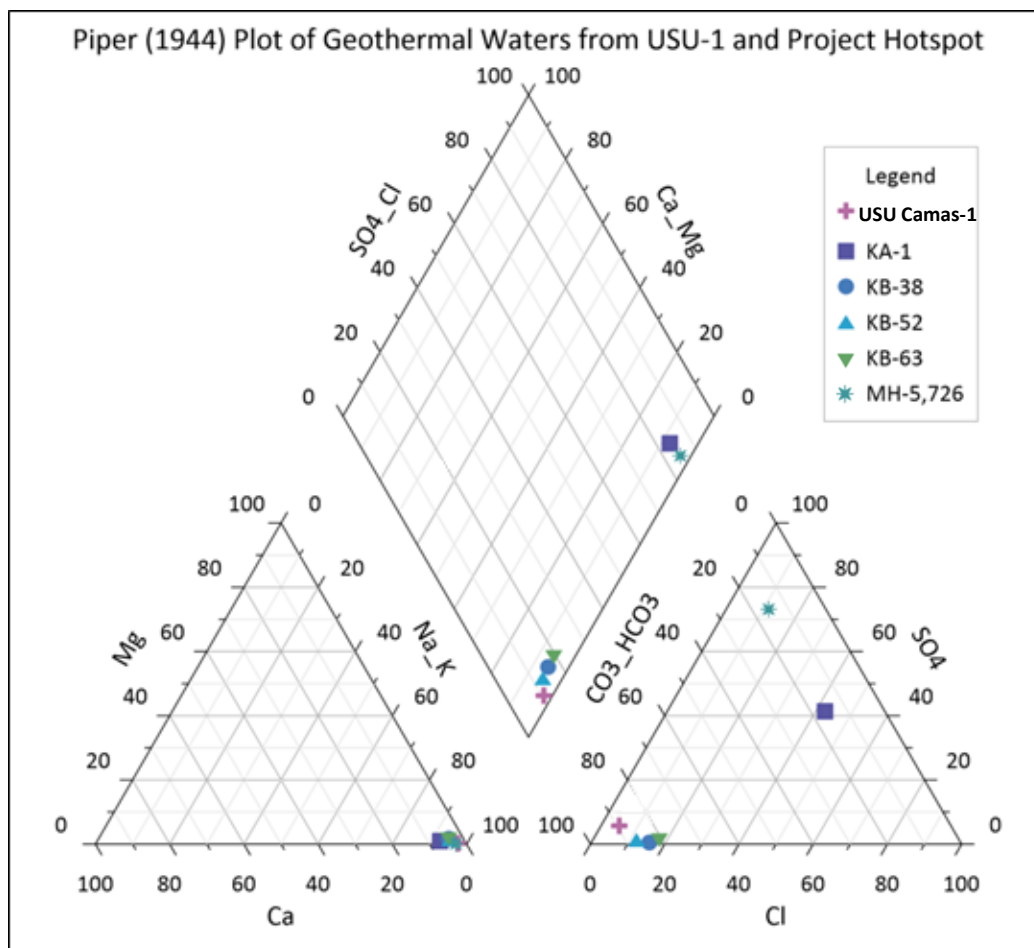
Figure 16. Piper (1944) diagram comparing major ion concentrations of the USU Camas-1 well water sample with Project Hotspot water samples (Freeman, 2013).

Stable Isotopes

Plotted $\delta^{18}O$ and δ^2H values of Camas Prairie water samples (Figure 17 and Table 4)

follow a trend below the global meteoric water line (GMWL) ($\delta^2H= 8*\delta^{18}O+10$; Craig, 1961).

Camas Creek Ranch surficial water samples have less negative $\delta^{18}O$ and δ^2H values, while the

USU Camas-1 water sample has more negative values. The general local trend seems to be that

higher temperatures correlate with lower isotopic ratios. This suggests that the system's water

input is meteoric in origin. This trend also supports the hypothesis of lateral flow entering the

well.
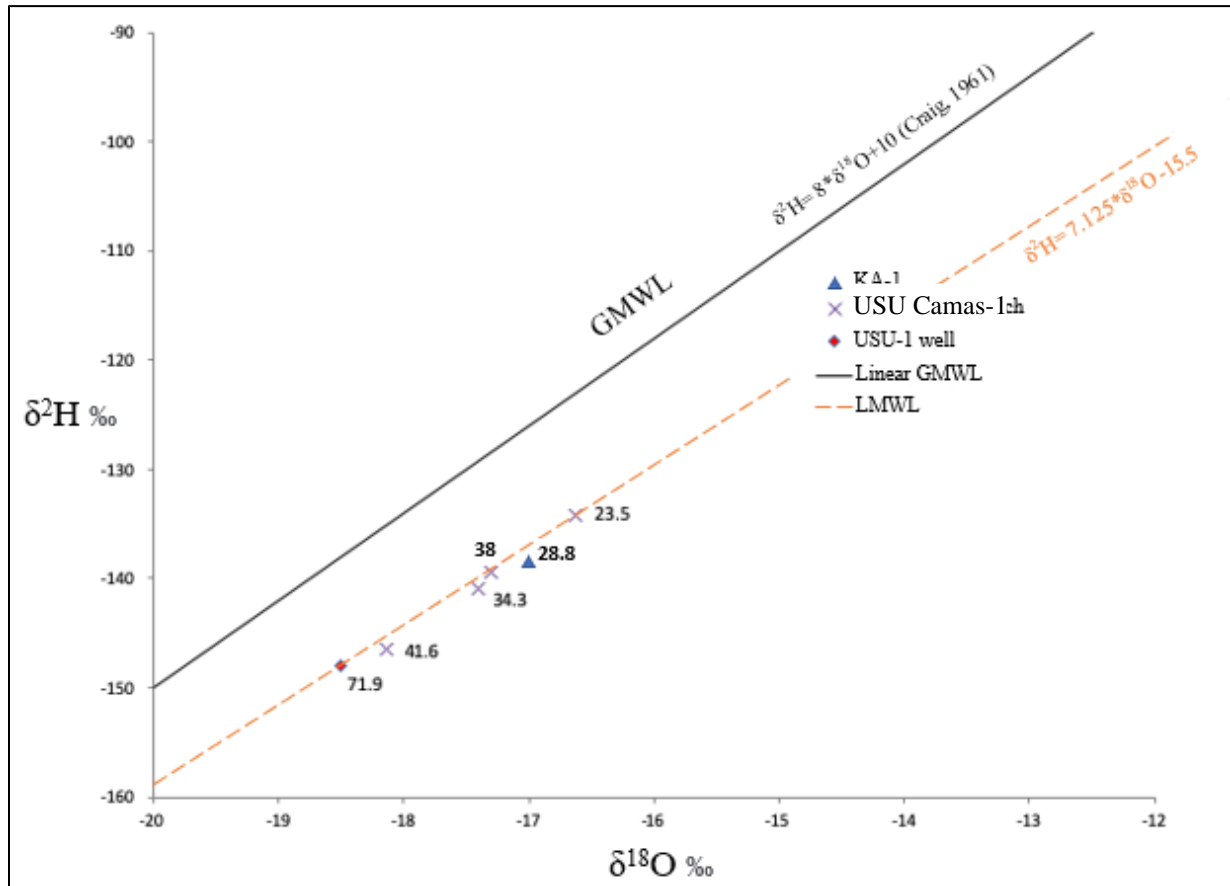
Figure 17. Deuterium (δ^2H) and oxygen-18 (δ^{18}O) isotope plot of Camas Prairie water samples plotted with the GMWL. The water sample from the USU Camas-1 well is marked with a red diamond. The Kimama sample (KA-1) is marked with a blue triangle. All samples are marked with measured temperatures in °C (adapted from the original plot created by Patrick Dobson).

Table 4. Deuterium (δ^2H) and oxygen-18 (δ^{18}O) values of USU Camas-1 and Project Hotspot well waters.

Sample	δ^{18}O (‰)	δ^2H (‰)
USU Camas-1	-18.5	-147.9
KA-1	-17.0	-141
MH-5,726	-3.2	-88

Comparing the results of the Project Hotspot isotope analyses (Freeman, 2013) with those of USU Camas-1 shows that the isotopic values of the USU Camas-1 well are similar to the shallow, meteoric water of the Kimama well. The isotopic values of both the USU Camas-1 and the Kimama water samples plot in line with the local meteoric water line (LMWL) ($\delta^2H=$ 7.125*$\delta^{18}O$-15.5) and near enough to the GMWL to thus be meteoric (Figure 17). The deeper water of the Mountain Home well contains less negative values of $\delta^{18}O$ and δ^2H, meaning its sample is less depleted in the heavier isotopes of ^{18}O and ^2H. Values of δ^2H and $\delta^{18}O$ in the Mountain Home sample show that its fluids are not meteoric since the isotopic values would plot well away from the GMWL. The Kimberly samples were not analyzed for stable isotopes of ^{18}O and ^2H due to cost constraints.

DISCUSSION

Geothermometry

The solubility of minerals used as geothermometers is a function of heat. In the range of 1-200 bars, pressure has a negligible effect on equilibration. Therefore, the two variables that dictate equilibration are the composition of the system and temperature (Arnórsson et al., 1983). Dissolution of rocks and secondary mineralization of the dissolved constituents are the two processes that are regulated by temperature and control mineral concentrations in fluids (Chou and Wollast, 1984; Holdren and Speyer, 1985). Assuming that the minimum required amount of each ion for each geothermometer is met and that the geothermal fluids are at least partially equilibrated, the concentrations of dissolved constituents in water samples can be evaluated and used in geothermometer equations to estimate reservoir temperature.

Geothermometer reservoir temperature calculations range between 82°C and 144°C, with a high consistency around 125°C (Table 5). The geothermometer equations used can be found in Table 1. The Giggenbach (1988) Na/K geothermometer produced the highest reservoir temperature calculation (144°C), while the Giggenbach (1988) K^2/Mg geothermometer produced the lowest temperature (81.8°C). This lowest calculated temperature is not much greater than the highest temperature measured in the well during temperature logging (80.3°C). The Fournier (1977) quartz geothermometer, the Fournier (1979) Na/K geothermometer, and the Fournier and Truesdell (1973) Na-K-Ca geothermometer produced consistent temperatures around ~125°C, while the Fournier (1977) chalcedony geothermometer and the Fournier and Potter (1979) Na-K-Ca-Mg geothermometer pair closely together at 98°C and 97°C, respectively.

Table 5. Calculated reservoir temperatures for USU Camas-1 and Project Hotspot wells (all temperatures reported in °C).

Well	Quartz Fournier 1977	Chalcedony Fournier 1977	Na/K Fournier 1979	Na/K Giggenbach 1988	Na-K-Ca Fournier & Truesdell 1973	Na-K-Ca-Mg Fournier & Potter 1979	K^2/Mg Giggenbach 1988
USU Camas-1	126	98	123	144	125	97	82
KB-38	134	107	135	155	142	86	80
KB-52	119	91	123	143	130	90	72
KB-63	123	95	120	140	130	83	73
MH-5,726	179	157	134	154	139	133	117
KA-1	164	141	143	163	139	125	80
KA-W	111	82	294	303	44	85	42

Certain geothermometers were developed with different facies of water and system compositions in mind. For instance, the Na-K-Ca geothermometer is more accurate for water that equilibrated at temperatures exceeding 100°C and for systems that have calcium-bearing minerals lining the walls of the well. Based on the results of the different geothermometers (Table 5), the USU Camas-1 system likely meets the first condition of the Na-K-Ca geothermometer and because much calcite is present in the system, it appears as if the Na-K-Ca is a reliable geothermometer for USU Camas-1. The Na-K-Ca and Na-K-Ca-Mg are examples of geothermometers that makes corrections to the older geothermometers to account for the presence of minerals that may affect the concentrations of other minerals used to calculate reservoir temperature. Therefore, there is bound to be a large spread of reservoir temperatures produced when using a suite of geothermometers. The classic geothermometers were selected to give an easy comparison between the USU Camas-1 and the Project Hotspot waters.

Today, the more accurate method is to use software such as iGeot that is designed to determine reservoir temperature using mineral saturation indices (Log Q/K). Nicolas Spycher

produced a convergence near 124°C with iGeoT software (Figure 18) using a dilution factor of

~2, a lower concentration of HCO_3 (97 mg/L), and chalcedony as the dominant form controlling

silica. The iGeoT software determines the dilution factor by analyzing sets of hydrochemical

conditions and selecting the one that produces the best clustering. In this case, the best cluster

was produced by a dilution factor of ~2, likely due to mixing with surface waters. Solubility

curves of various minerals converge on the point at ~124°C with tight agreement. This agrees

with the three traditional geothermometers that produced reservoir temperatures ranging from

123°C to 126°C (Table 5).
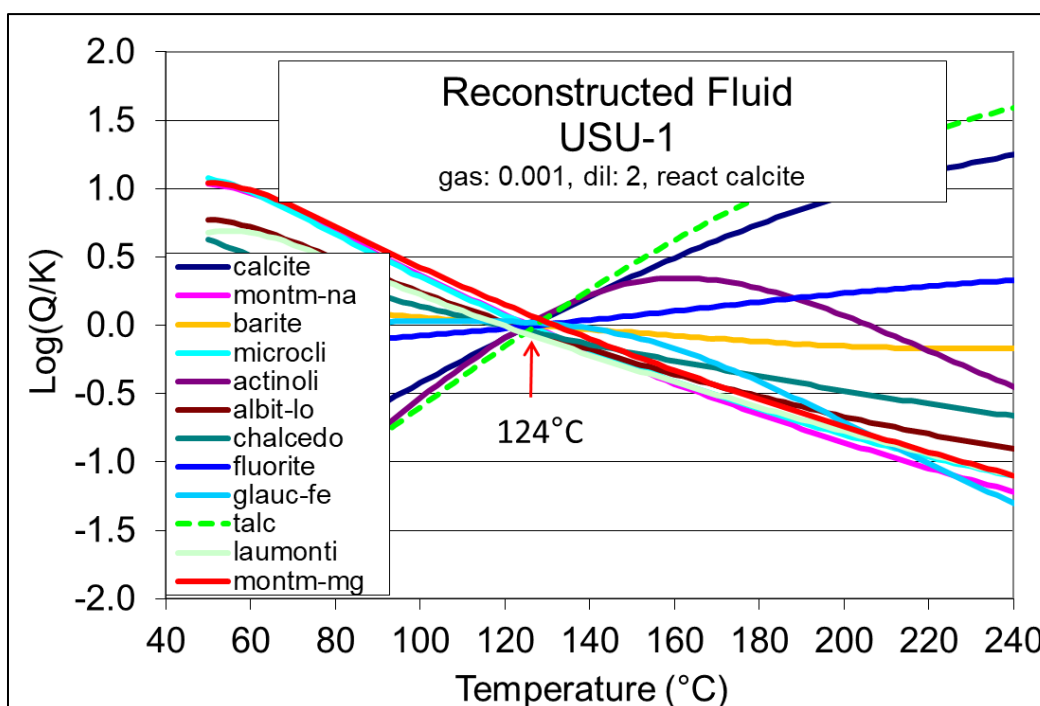
Figure 18. Geothermometer clustering plot created by Nicolas Spycher using his software known
as iGeoT. USU-1 refers to USU Camas-1.

To determine if the USU Camas-1 well fluid is fully equilibrated, partially equilibrated,

or immature, calculated reservoir temperatures of 81.8°C and 143.5°C produced by the

geothermometers of K^2/Mg and Na/K (Giggenbach, 1988), respectively, were plotted on a

Giggenbach (1988) ternary diagram (Figure 19). Waters categorized as immature are unsuitable

for geothermometric analysis. The USU Camas-1 sample plots in the partially equilibrated area

of the diagram and far enough away from the Mg point to be an acceptable candidate for

geothermometry. True equilibration only takes place in systems under stagnant conditions over

an infinite period of time (Giggenbach, 1984). Therefore, samples almost never plot on the full

equilibrium line.
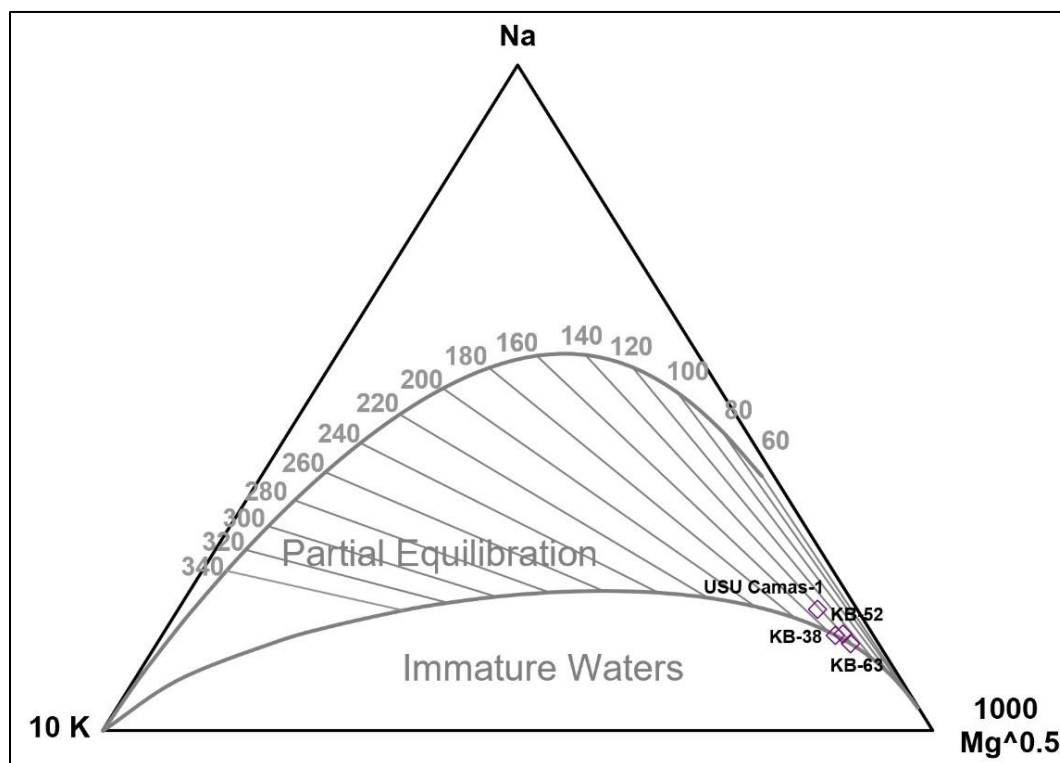
Figure 19. Giggenbach (1988) plot of the USU Camas-1 and Kimberly water samples.

The ternary diagram in Figure 20 is used as a general way to categorize waters into three

broad groups: chloride dominant mature waters, sulfate dominant steam-heated waters, and

bicarbonate dominant peripheral waters (Giggenbach, 1988). The dominant bicarbonate presence

in the USU Camas-1 sample explains its higher pH (Table 3), and its heightened Na:K ratio that

is akin to those of the Soda Springs (peripheral) waters (Giggenbach, 1988). The lower acidity in

Soda Springs waters allows for the formation of aluminum silicates. Potassium is removed from

the geothermal fluids and incorporated into K-rich clays. While this phenomenon integrates

potassium into the formation, sodium remains suspended in the geothermal fluids (Giggenbach, 1988). Water that has interacted with the Idaho batholith also tends to have elevated pH values and fluoride content (Mitchell, 1976).
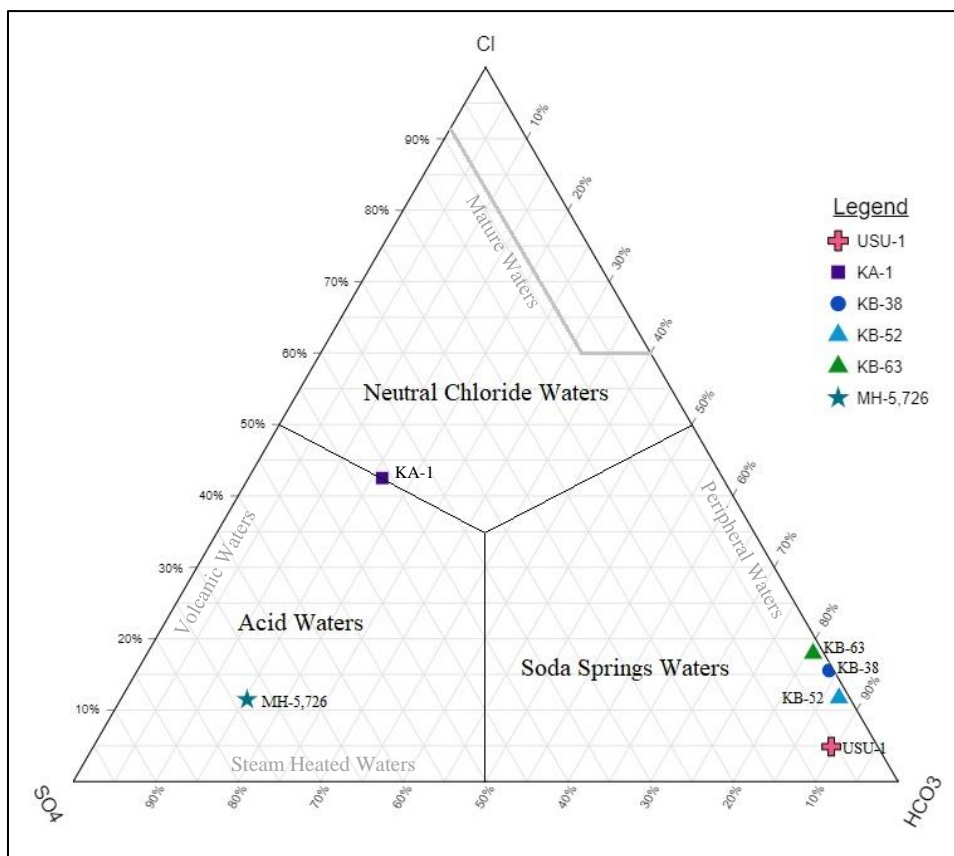
Figure 20. USU Camas-1 and Project Hotspot water samples plotted on a ternary diagram of the three major anions (Giggenbach, 1988). USU-1 refers to USU Camas-1.

Proportionally, the Kimberly samples are similar to USU Camas-1 in that they are dominated by bicarbonate and thus plot in the Soda Springs waters section. The Kimama sample plots on the cusp of the steam-heated acid waters and the neutral chloride/mature waters, for it has nearly equal parts chloride and sulfate. The Mountain Home sample is dominated by sulfate, so it plots in the acid water (steam heated) section of the diagram (Freeman, 2013).

Hydrochemical Properties

The sodium-bicarbonate dominant USU Camas-1 water is similar chemically to the Kimberly water (Table 2), and produced similar reservoir temperature calculations (Table 5). The quartz (Fournier, 1977) and Na/K (Fournier, 1979) geothermometers yielded reservoir temperatures of around 125°C for both wells. On the Giggenbach (1988) ternary diagram of the three major anions, the Kimberly samples all plot on the Soda Springs (peripheral) waters section, as does the USU Camas-1 water sample (Figure 20). This is due to the dominant proportion of bicarbonate in each sample. In Figure 16, the USU Camas-1 and Kimberly samples plot as a cluster on the sodium-bicarbonate facies of the Piper (1944) plot. Water samples from both wells are in partial equilibrium as they plot in this zone on the Giggenbach (1988) maturity diagram (Figure 19). On the basis of major ion concentrations, the two wells produce very similar waters.

It is curious that the hotter, deeper systems in the region have lower $\delta^{18}O$ and δ^2D values (Figure 17), since geothermal fluids at depth would be expected to react with the surrounding rocks and produce less negative isotopic values than shallower systems. In other words, deeper, hotter waters typically are less depleted in $\delta^{18}O$ and δ^2D compared to cooler waters at the surface.

One possible explanation is that a separate, deeper flow system is present and is being supplied by recharge from the north. The peak of Smoky Dome of the Soldier Mountains has an elevation of 3,077 m (10,095 ft) asl and is located ~20.3 km (12.6 mi) north of USU Camas-1, which rests at an altitude of 1,545 m (5,069 ft) asl. The nearest peak that shares a ridgeline with Smoky Dome is located slightly nearer USU Camas-1 at ~18.2 km (11.3 mi) and has an elevation of 2,790 m (9,150 ft) asl. The nearest foothills of the Soldier Mountains are located

~10.2 km (6.3 mi) away from the USU Camas-1 well and have altitudes ranging between ~1,800 m and 2,115 m (5,900 and 6,939 ft) asl.

Another explanation could be that the Mount Bennett Hills are acting as the recharge zone for the geothermal fluids of the USU Camas-1 well. Davis Mountain, located ~11 km (7 mi) south of the USU Camas-1 well, reaches a maximum altitude of 2,077 m (6,814 ft) asl. The distance between the peak of Davis Mountain and USU Camas-1 is nearly half that from the peak of Smoky Dome to USU Camas-1 but only ~0.8 km (0.5 mi) further than the distance between the foothills and the well.

Yet another explanation would be that the fluids of the system precipitated during the late Pleistocene under a climate that was colder and wetter than the one present in the region today. This hypothesis was suggested by Flynn and Buchanan (1990) for the Great Basin region lying to the south of the Camas Prairie. The system also simply might not be hot enough or have a long enough residence time for the waters to uptake relatively high concentrations of ^{18}O and ^{2}H.

Permeable Zone and Lateral Flow

Geophysical logs of SP, resistivity, and conductivity experience fluctuations at the approximate depth of the productive zone at ~346.9 m (1,138 ft) bgs (Figure 10). Resistivity drops to nearly zero ohm-m, while SP and conductivity each spike. At this depth, there is an inflection point in the temperature profile, suggesting that geothermal fluids are entering the well. It was during the drill run that advanced to this depth that the drillers reported encountering a productive zone.

Temperature logs following shortly after the injection of cold water into the well suggest that the permeable zone extends deeper than just the productive zone at ~346.9 m (1,138) bgs

(Figure 12). The temperature profile begins to decline at a depth of ~357.5 m (1,173 ft) bgs 14 hours after the injection of cold water, indicating that the injected water was integrated into the formation at this depth. The acceptance of cold water at ~357.5 m (1,173 ft) bgs is likely due to the formation being relatively more permeable there than at other depths. The next temperature log, occurring 59 days after injection, shows a rebound in the profile of the well. The sharp decline in temperature that was centered at ~357.5 m (1,173 ft) bgs and clearly visible in the 14-hour log is much less prominent and nearly isothermal. Fifty-nine days following injection, warmer geothermal fluids had displaced the colder injection water and/or equilibrated with it. The permeable section that Garg and Goranson (2018) hypothesized is corroborated by a similar change in temperature centered at 356.6 m (1,170 ft) bgs (Figure 10) recorded during the third geophysical run.

Using a Horner plot, Garg and Goranson (2018) were able to estimate the USU Camas-1 well's transmissivity as ~0.1-0.4 cm^2/s (9-36 ft^2/d). The modest transmissivity likely means the permeability is relatively high between ~346.9 and 357.5 m (1,138 and 1,173 ft) bgs. A seasonal artesian flow rate (~0.7 L/s) observed from the well further supports the presence of a permeable zone intersected by the well.

Temperatures remaining constant below 353.6 m (1,160 ft) bgs (Figure 11) suggest that geothermal fluids are not flowing into the well below this point. A homoclinal geothermal gradient would indicate that water is entering the bottom of the borehole, but the presence instead of an isothermal gradient below the productive zone suggests that the well intersected no faults in the lower section that supply the well with geothermal fluids.

The presence of a seasonal artesian flow also indicates lateral flow at depth, likely through the permeable zone. Seasonal recharge from the higher altitudes of the Soldier

Mountains to the north or the Mount Bennett Hills to the south may cause the artesian flow of the USU Camas-1 well as discussed above. As snowmelt percolates into the system, pressure in the well would build until surface flow could be observed.

Upwelling Zone

Nearby wells were logged for temperature at various times between 2010 and 2019, mainly by Roy Mink. Well conditions (i.e., time elapsed since shut in) are not well known for all wells. Wells are categorized as either hot or cold based on their maximum temperatures. All cold wells exhibit maximum temperatures less than 30°C, while all hot wells boast maximum temperatures greater than 60°C. The temperature profiles of all cold wells (1A, 3A, and SRV-2) are plotted in Figure 21. The highest temperature measured in the cold wells (29°C) occurred in 1A at a depth of 16 m (52.5 ft). The lowest temperature measured in the cold wells (9.9°C) occurred in 3A at a depth of 24 m (78.7 ft). The cold wells all drop in temperature with depth at first. Well 1A reverses this trend by increasing with depth below ~54 m (177 ft) as does 3A near its TD at ~73 m (240 ft). Well SVR-2 does not follow this trend.

The temperature profiles of hot wells (USU Camas-1, Barron, Gonsales, and Barron Big Hot Spring) presented in Figure 22 illustrate a few trends shared between some of the wells. The Barron well reaches its maximum temperature (90.6°C on 7/22/10 and 86.7°C on 8/8/16) at a depth of 91.4 m (300 ft) in both runs. The Barron run that occurred on 8/8/16 shows a BHT rebound to 85.0°C at a depth of 160 m (525 ft) from 81.1°C at a depth of 152.4 m (500 ft). The Barron run on 7/22/10 does not show a similar spike in BHT. The profile of the USU Camas-1 run on 12/22/18 reflects the two Barron runs closely with a spike in temperature to 80°C centered at a depth of 76.2 m (250 ft). At a depth of 338.3 m (1,110 ft) the USU Camas-1 well reached its maximum temperature of 81.2°C. This is also the maximum temperature recorded

during the 7/9/19 run for USU Camas-1 between the depths of 289.6 and 350.5 m. This value is slightly higher than the maximum temperature recorded during the temperature log run on 10/24/19 (Figure 11). It would be illuminating to see if the water at greater depths at the
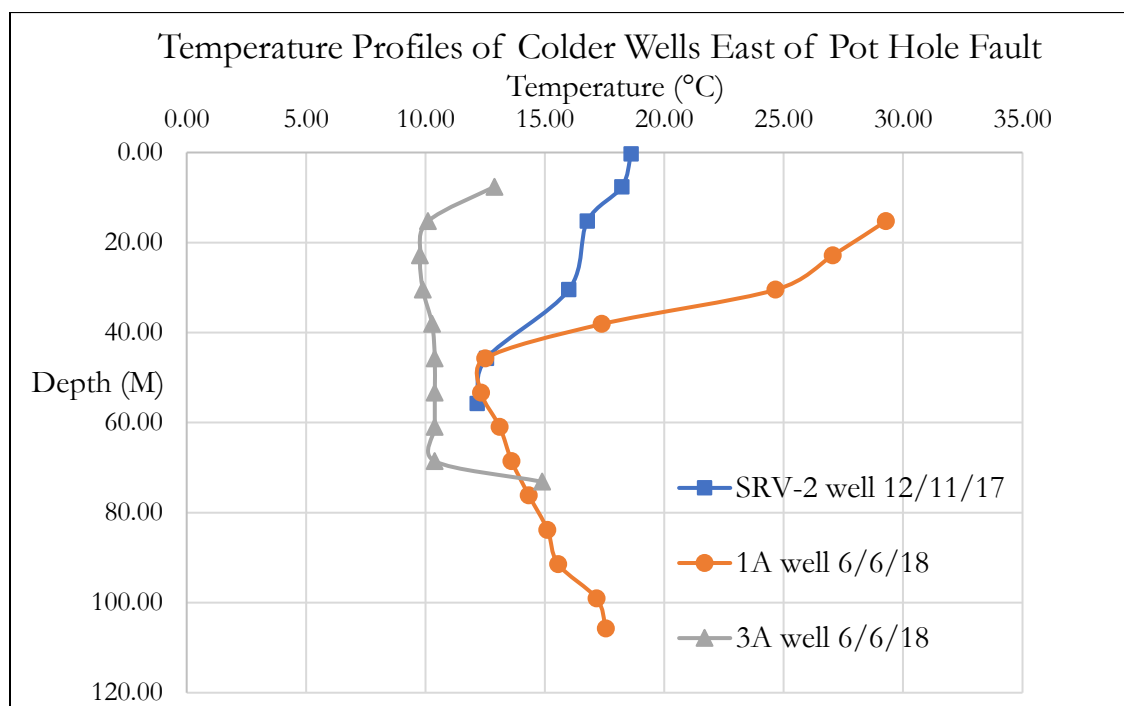

Figure 21. Temperature profiles of colder wells of the Camas Prairie east of the Pothole fault.

location of the Barron well follows the same trend that USU Camas-1 does of first rapidly increasing in temperature to a point near its maximum, then decreasing slightly, only to increase to its true maximum temperature. The Gonsales well does not follow the Barron runs as closely as the USU Camas-1 run on 12/22/18 does. This is perplexing considering that the Gonsales well is located significantly closer to the Barron well. The Barron Big Hot Spring well, in addition to having the coldest maximum temperature of the hot wells of 67.2°C at 45.7 m (150 ft), is also the shallowest one. Of all the hot wells, the USU Camas-1 temperature run on 7/9/19 is the only one to begin with a high temperature at the ground surface (61.7°C). This is to be expected because

the well was flowing. All other hot wells begin with temperatures less than 20°C at the ground surface, including the USU Camas-1 run on 12/22/18 when it was not flowing.
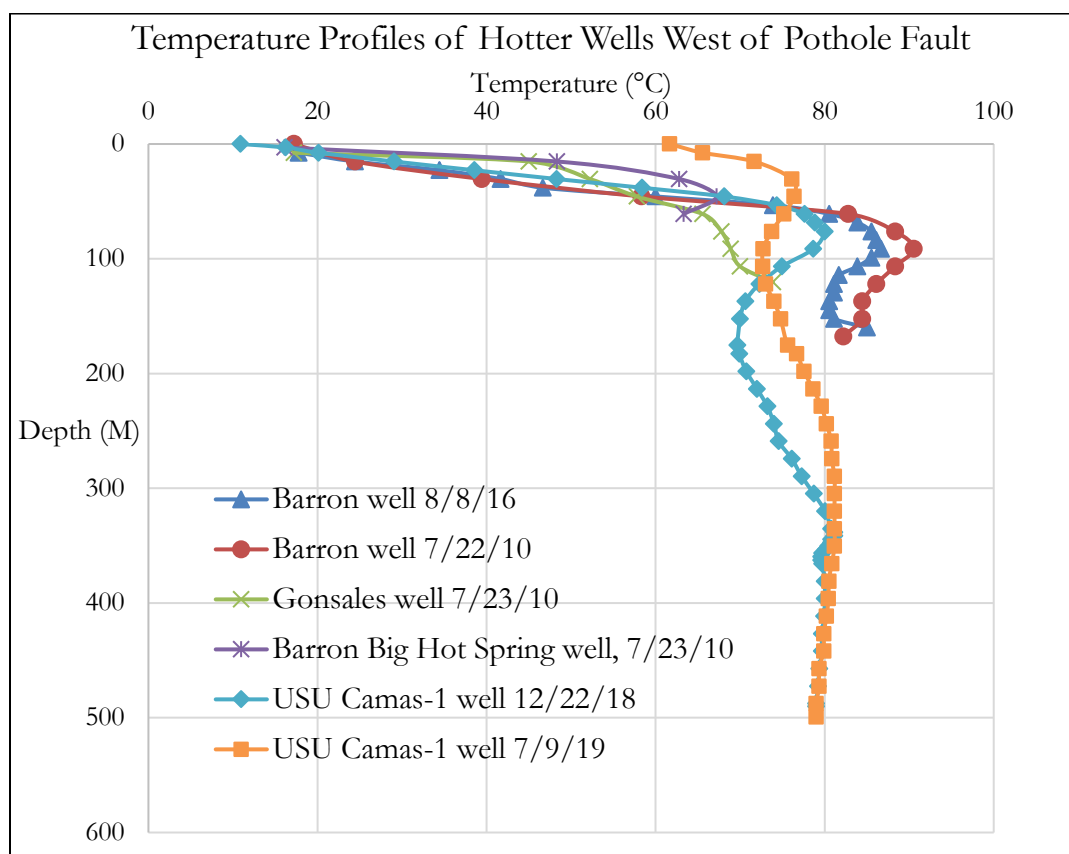
Figure 22. Temperature profiles of hotter wells of the Camas Prairie west of the Pothole Fault.

By mapping the locations of hot and cold wells (Figure 23), one can delineate the path of geothermal fluid flow. Figure 23 shows a ~0.7 km (0.44 mi) distance between the Gonsales well and the SVR-5 well. These are the two hot and cold wells located nearest to each other. It is at a point between the two wells that the source supplying the hot wells terminates. It appears that geothermal fluids are flowing northward from the Mount Bennett Hills area as the hot wells are located to the south of the cold wells (Figure 23), and that the Pothole fault is conducting the geothermal fluids. The hot wells are located nearer to and generally west of the Pothole fault, as

depicted by Shervais et al. (2017), while the cold wells are located well to the east of the fault.

The Gonsales well is the exception in that it lies slightly east of the Pothole fault.
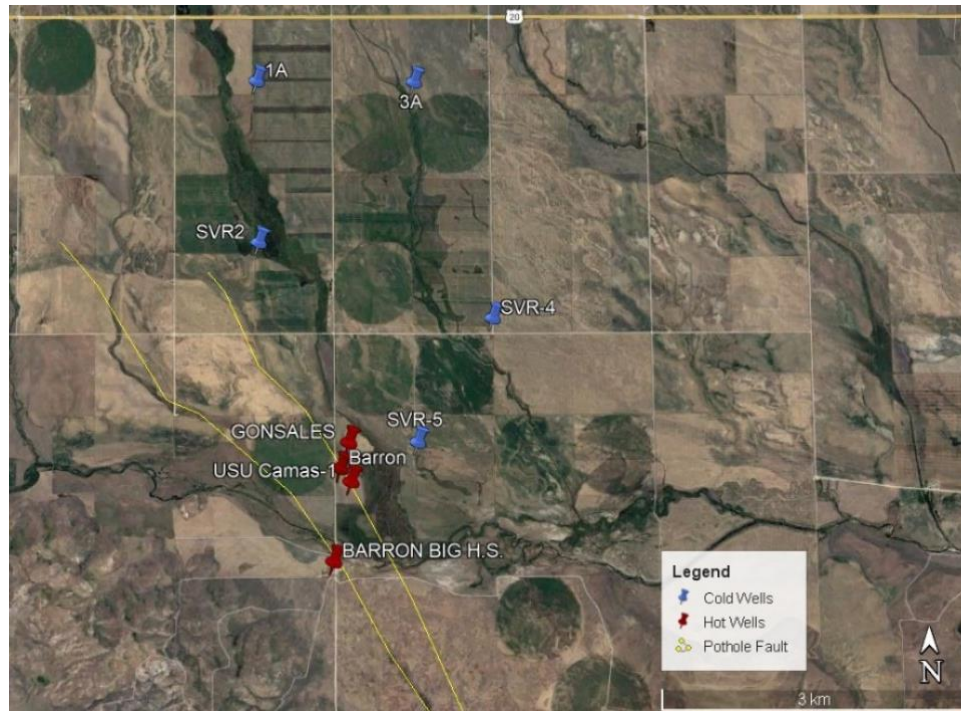

Figure 23. Map of the Camas Prairie depicting hot and cold well locations, as well as the orientation of the Pothole fault per Shervais et al. (2017).

SUMMARY, CONCLUSIONS AND RECOMMENDATIONS

Summary

The Camas Prairie was identified as a model location for geothermal exploration and was selected for drilling to validate the GPFA, the approach used to identify the Camas Prairie as a potential high-temperature geothermal resource. The GPFA utilizes the stacking of geospatial data including: the presence of local hot springs and hot water wells, MT data suggesting the presence of a clay seal, fault networks, young volcanics, high ^{3}He/^{4}He ratios, and estimated reservoir temperatures up to 200°C. The USU Camas-1 well was drilled via rotary methods to a depth of ~491.3 m (1,612 ft) bgs, and extended to a TD of ~618.3 m (2,028.5 ft) bgs via coring.

The lithologic log (Figure 10) was constructed based on XRD results and in-field reports of cuttings and core. Valley fill sediment occupied the upper 314 m (1,030 ft) of the borehole. Granite of the Idaho batholith, rhyolite of the Challis volcanics, and clay gouges rested under the sediments. Review of the cuttings revealed that an instance of mineralization was encountered between 344.4-347.5 m (1,130-1,140 ft) bgs, supporting the hypothesis of geothermal fluids circulating in this range. Drill reports detailing a productive zone encountered at a depth of ~346.9 m (1,138 ft) bgs further support this hypothesis. XRD results of the core revealed that there are hydrothermal alteration facies, such as chlorite, gobbinsite, and clay gouge, present throughout the length of the USU Camas-1 well below the productive zone. This is another indicator of previous geothermal fluid circulation.

Geophysical logs of SP, resistivity, conductivity, gamma ray, and delta t (Figure 10) allow for the establishment of formation characteristics. Resistivity remains low throughout the sediment section of the well, but rises once the underlying basement igneous rocks are reached. A similar response can be observed in the conductivity profile with some troughs and peaks

opposing those of resistivity. SP increases and decreases opposing resistivity as well, but does so throughout the entire length of USU Camas-1 that was logged, down to a depth of 492.3 m (1,615 ft). Elevated gamma ray readings correlate with the presence of rhyolite due to the high content of potassium feldspar, and delta t has a high amplitude with many peaks throughout the length of the well. The peaks and troughs in the geophysical logs of resistivity, conductivity, and SP support the existence of a productive zone near ~346.9 m (1,138 ft) bgs. Measures of relatively low resistivity and high SP and conductivity suggest that the formation is permeable at this depth. Gamma ray increases near 347.5 m (1,140 ft) bgs due to the contact between the overlying granite and underlying rhyolite at this depth, while delta t peaks at ~ 346.9 m (1,138 ft) bgs to ~375 μsec/ft then decreases to fluctuate between ~50 and 200 μsec/ft near 347.5 m (1,140 ft) bgs.

Temperature rapidly increases at the depth of the productive zone at 346.9 m (1,138 ft) bgs suggesting the flow of hot geothermal fluids (Figure 10). The maximum temperature recorded in the USU Camas-1 well was 80.3°C (Figure 11), which was encountered at ~353.6 m (1,160 ft), about 4 m above the approximate depth of the permeable zone that accepted cold injected water at ~357.5 m (1,173 ft) bgs. The temperature profile (Figure 11) shows that below the productive zone, fluids are mostly isothermal and the temperature even decreases slightly with depth; this makes it difficult to calculate a geothermal gradient as it appears that lateral flow is entering the well. The USU Camas-1 well is cased and cemented to a depth of 346.9 m (1,138 ft) and thus an upper gradient expresses itself from the surface to this depth (169°C/km). Since the well is isothermal below this point, the gradient is effectively 0°C/km.

Results of the injection test conducted and analyzed by Garg and Goranson (2018) produced transmissivity values of ~0.1-0.4 cm^2/sec (9 and 36 ft^2/day). Due to an anomaly in the

pressure data, the falling limb was used to calculate transmissivity. The first temperature log

taken shortly after the injection of cold water shows a dip in temperature centered at ~357.5 m

(1,173 ft) (Figure 12), indicating a permeable zone that assimilated cold injected water at this

depth.

Water chemistry of the USU Camas-1 sample consisted of measuring concentrations of

major ions and stable isotopes of ^{18}O and ^{2}H. Analysis of the major ions of the USU Camas-1

sample show that the water is dominated by sodium and bicarbonate. Rendering all major ions

graphically, the USU Camas-1 sample plots in the same region of the Piper (1944) diagram as all

but two of the other Camas Prairie samples of Mattson et al. (2016) and the Kimberly samples of

Project Hotspot, but not Kimama or Mountain Home (Figures 15 and 16). Plotting the USU

Camas-1 and Hotspot water samples on a ternary diagram of the three major anions provides a

graphical representation of the well waters (Figure 20). The USU Camas-1 and Kimberly

samples plot on the Soda Springs (peripheral) waters section of the diagram, for they are

dominated by bicarbonate. Mountain Home plots on the acid water (steam-heated) section, for it

is dominated by sulfate. Kimama plots on the interface between the acid water and neutral

chloride (mature) waters, for it is composed of nearly equal parts sulfate and chloride. The USU

Camas-1 stable isotope ratios of ^{18}O and ^{2}H plot (Figure 17) with other local samples and

Kimama on a LMWL that trends below the GMWL (Craig, 1961) and is represented by the

equation $\delta^2H=7.125*\delta^{18}O-15.5$. This indicates that the water of the Camas Prairie has a meteoric

component. Also, there appears to be a correlation between temperature and isotope values;

hotter water samples have more negative isotopic values, while colder water samples have less

negative values of ^{18}O and ^{2}H. The Mountain Home sample contained $\delta^{18}O$ and δ^2H values that

plot far below the LMWL and to the right of the other samples.

Geothermometry calculations suggest that the Camas Prairie has a reservoir temperature ranging from 81.8-143.5°C with consistency around ~125°C (Table 5). The results of Nicolas Spycher's iGeot software support the reservoir temperature being near 125°C with a cluster generated at 124°C (Figure 18). Rendering the Giggenbach (1988) Na/K and the Giggenbach (1988) K^2/Mg geothermometers graphically determined that the USU Camas-1 water sample is partially equilibrated and thus an adequate candidate for geothermometry (Figure 19). The chemistry between USU Camas-1 and Kimberly is similar (Figure 16), and their calculated reservoir temperatures are similar as well. The calculated reservoir temperatures of the KB-52 and KB-63 samples consistently fell within 10°C of the USU Camas-1 temperatures. The calculated reservoir temperatures of the KB-38 sample were consistently higher than the USU Camas-1 and other Kimberly samples.

Conclusions

The presence of a permeable zone at a depth of ~352.5±5 m (1,156±16 ft) bgs is supported by: (1) the maximum temperature of the borehole reached at this depth (~80.3°C), (2) suppressed temperatures measured at this depth following injection of cold water, and (3) spikes in geophysical data near this depth. There is some discrepancy as to the exact depth of the permeable zone. Geophysical spikes suggest it is located near a depth of ~347.5 m (1,140 ft), while the zone that accepted cold injected water is centered at ~357.5 m (1,173 ft). It is likely that the productive zone is located at the shallower depth of ~347.5 m (1,140 ft), and that there is another permeable zone beneath it at ~357.5 m (1,173 ft).

The necessary components of a geothermal system (heat, water, permeability, and a clay seal) are present in the Camas Prairie. The two most obvious components of a geothermal system, water and heat, are clearly present. The well was observed flowing artesian at the time of

sampling, and temperatures as high as 80.3°C were measured in the USU Camas-1 well. The two

mapped fault systems converging on the Camas Prairie are evident in the core with prevalent

fractures and low recovery rates suggesting void space and thus permeability. Moderate

transmissivity values of ~0.1-0.4 cm^2/s (9-36 ft^2/d) determined by the pressure test and the ~0.7

L/s flow rate at the time of sampling further corroborate high permeability. MT data suggesting

the presence of a clay seal are confirmed by sandy clay, clayey sand, and clay layers in the

overlying sediments encountered in the cuttings at depths of 268-314 m (880-1,030 ft) (Figure

10).

The Camas Prairie is a promising area in terms of geothermal reservoir features, but it

does not boast the same level of promise as Mountain Home or Kimama based on temperature

data and calculated reservoir temperatures. The maximum temperature measured is higher for

Mountain Home (140°C) than USU Camas-1 (80.3°C). While the Kimama well's maximum

temperature (59.3°C) is less than that of USU Camas-1, its estimated reservoir temperatures are

greater than those of USU Camas-1. Kimberly and USU Camas-1 likely have similar reservoir

temperatures based on their categorization under the same hydrochemical facies of the Piper

(1944) and two Giggenbach (1988) diagrams (Figures 16, 19, and 20), and their similar

geothermometer results. Given the geothermometer results (Table 5) and Nicolas Spycher's

analysis (Figure 18) the temperature of the reservoir in which the USU Camas-1 water

equilibrated is likely ~125°C, while the reservoir temperature for Kimberly is likely ~130°C.

Based on the map of cold and hot wells (Figure 23) the colder wells are located further

north than the hotter wells, and to the east of and further away from the Pothole fault. It appears

that the geothermal fluid is flowing from the Mount Bennett Hills to the south of the Camas

Prairie, potentially via the Pothole fault. Recent ^{40}Ar-^{39}Ar dating of the Pothole basalt by

Shervais et al., (2017) produced an age of 692.1 ±20.9 ka; by the principle of crosscutting, this determines that the Pothole fault system, as well as the range-front fault along the north margin of the Mount Bennett Hills, were active during the late Pleistocene. Given the presence of these young basalts and that water samples analyzed previously contained elevated ^{3}He/^{4}He ratios (Dobson et al., 2015), the heat source of the Camas Prairie is likely a magmatic one. While the magmatic source is likely controlling heat input to the system, it also may be possible that the range-front fault along the north margin of the Mount Bennett Hills and/or the Pothole fault is/are acting as the conduit for geothermal fluids at great depth to rise to the surface without a magmatic source being present.

Recommendations

The geothermal potential of the Camas Prairie is such that it is adequate for low-temperature geothermal purposes, but the fluids are not hot enough to be developed as a high-temperature resource. The highest temperature recorded in the well (~80.3°C) is well below the high-temperature threshold of 150°C, and even the highest calculated reservoir temperature (143.5°C) still falls short of this threshold. The isothermal nature of the USU Camas-1 well's temperature profile below the productive zone leads to the same conclusion.

USU Camas-1 was, and any future geothermal exploration wells should be, located north of the range-front fault along the north margin of the Mount Bennett Hills, preferably near the intersection of that fault with the Pothole fault. It would have been preferable not to drill USU Camas-1 vertically, but inclined at an angle to increase the odds of encountering one or both of these faults. Any future geothermal exploration wells drilled in the area likewise should be drilled at an angle instead of vertically.

REFERENCES

Arnórsson, S., 1978, Major element chemistry of the geothermal sea water at Reykjanes and Svartsengi, Iceland: Mineralogical Magazine, v. 42, p. 209-220.

Arnórsson, S., Gunnlaugsson, E., and Svavarsson, H., 1983, The chemistry of geothermal waters in Iceland. II. Mineral equilibria and independent variables controlling water compositions: Geochimica et Cosmochimica Acta, v. 47, p. 547-566.

Blackwell, D.D., 1989, Regional implications of heat flow of the Snake River Plain, Northwestern United States: Tectonophysics, v. 164, p. 323-343.

Blackwell, D.D., and Richards, M., 2004, Geothermal map of North America: American Association of Petroleum Geologists, scale 1:6,500,000, 1 sheet.

Chadwick, D.J., Payne, S.J., Hove, T.V., and Rodgers, D.W., 2007, Contemporary tectonic motion of the eastern Snake River Plain: A campaign global positioning system study: Tectonics, v. 26, p. 1-7.

Chou, L., and Wollast, R., 1984, Study of the weathering of albite at room temperature and pressure with a fluidized bed reactor: Geochimica et Cosmochimica Acta, v. 48, p. 2205-2217.

Clemens, D.M., and Wood, S.H., 1993, Late Cenozoic volcanic stratigraphy and geochronology of the Mount Bennett Hills, central Snake River Plain, Idaho: Isochron West, no. 60, p. 3-14.

Cumming, W., 2016, Resource conceptual models of volcano-hosted geothermal reservoirs for exploration well targeting and resource capacity assessment: Construction, pitfalls and challenges: Geothermal Resources Council Transactions, v. 40, p. 623-637.

Craig, H., 1961, Isotopic variations in meteoric waters: Science, v. 133, p. 1702-1703

Dobson, P.F., Kennedy, B.M., Conrad, M.E., McLing, T.L., Mattson, E.D., Wood, T.R., Cannon, C.J., Spackman, R., van Soest, M., and Robertson, M., 2015, He isotopic evidence for undiscovered geothermal systems in the Snake River Plain, in Proceedings, 40th Workshop on Geothermal Reservoir Engineering: Palo Alto, Stanford University, p. 1-5.

Ellis, A.J., 1970, Quantitative interpretation of chemical characteristics of hydrothermal systems: Geothermics, v. 2, p. 516-528.

Ellis, A.J., 1971, Magnesium ion concentrations in the presence of magnesium chlorite, calcite, carbon dioxide, quartz: American Journal of Science, v. 271, p. 481-489.

Fazal, M.R., and Kamran, M., 2021, Renewable Energy Conversion Systems: Academic Press, p. 265-281.

Ferguson, G., Grasby, S.E., and Hindle, S.R., 2009, What do aqueous geothermometers really tell us?: Geofluids, v. 9, p. 39-40.

Flynn, T., and Buchanan, P.K., 1990. Geothermal fluid genesis in the Great Basin: U.S. Department of Energy, p. 1-30.

Fournier, R.O., 1977, Chemical geothermometers and mixing models for geothermal systems: Geothermics, v. 5, p. 41-50.

Fournier, R.O., 1979, A revised equation for Na-K geothermometer: Geothermal Resources Council Transactions, v. 3, p. 221-224.

Fournier, R.O., and Potter, R.W., 1979, Magnesium correction to the Na-K-Ca chemical geothermometer: Geochimica et Cosmochimica Acta, v. 43, p. 1543-1550.

Fournier, R.O., and Truesdell, A., 1973, An empirical Na-K-Ca geothermometer for natural waters: Geochimica et Cosmochimica Acta, v. 37, no. 5, p. 1255-1275.

Fournier, R.O., White, D.E., and Truesdell, A., 1974, Geochemical indicators of subsurface temperature – Part 1, Basic assumptions: U.S. Geological Survey, Open-File Report 74-1033, p. 259-262.

Freeman, T.G., 2013, Evaluation of the Geothermal Potential of the Snake River Plain, Idaho, Based on Three Exploration Holes [M.S. thesis]: Logan, Utah State University, p. 1-66.

Garg, S.K., and Goranson, C., 2018, Analysis of downhole data from USU Camas-1 well: Utah State University, p. 1-9.

Gaschnig, R.M., Vervoort, J.D., Lewis, R.S., and Tikoff, B., 2011, Isotopic evolution of the Idaho batholith and Challis intrusive province, northern US Cordillera: Journal of Petrology, v. 52, no. 12, p. 2397–2429.

Giggenbach, W.F., 1984, Mass transfer in hydrothermal alteration systems – A conceptual approach: Geochimica et Cosmochimica Acta, v. 14, p. 2693-2711.

Giggenbach, W.F., 1988, Geothermal solute equilibria: Derivation of Na–K–Mg–Ca geoindicators: Geochimica et Cosmochimica Acta, v. 52, p. 2749-2765.

Glen, J.M., Liberty, L.M., Gasperikova, E., Siler, D., Shervais J.H., Ritzinger, B., Athens, N., and Earney, T., 2017, Geophysical investigations and structural framework of geothermal systems in west and southcentral Idaho, Camas Prairie to Mountain Home, in Proceedings, 41st Workshop on Geothermal Reservoir Engineering: Palo Alto, Stanford University, p. 11.

Holdren, G.R., and Speyer, P.M., 1985, pH dependent changes in the rates and stoichiometry of dissolution of an alkali feldspar at room temperature: American Journal of Science, v. 285, p. 994-1026.

Holmes, A., 1925, Radioactivity and the earth's thermal history, Part II: Geologic Magazine, v. 2, p. 60-71.

Honjo, N., 1990, Geology and stratigraphy of the Mount Bennett Hills, and the origin of west-central Snake River Plain rhyolites [Ph.D. dissertation]: Houston, Rice University, p. 259.

Kiilsgaard, T.H., and Lewis, R.S., 1985, Plutonic rocks of Cretaceous age and faults in the Atlanta lobe of the Idaho batholith, Challis Quadrangle, in Proceedings, Symposium on the Geology and Mineral Deposits of the Challis 1°x2° Quadrangle, Idaho: Spokane, Washington Geological Survey Bulletin 1658, p. 29-42.

Lewis, R.S., and Kiilsgaard, T.H., 1991, Eocene plutonic rocks in south central Idaho: Journal of Geophysical Research, v. 96, p. 13,295-13,310.

Li, J., Sagoe, G., and Li, Y., 2020, Applicability and limitations of potassium-related classical geothermometers for crystalline basement reservoirs: Geothermics, v. 84, p. 1-8.

Mahon, W.A.J., 1965, Calcium and magnesium in the natural thermal waters of New Zealand: New Zealand Journal of Science, v. 8, p. 66.

Malde, H.E., 1959, Fault zone along northern boundary of western Snake River Plain, Idaho: Science, v. 130, p. 272.

Marini, L., 2000, Geochemical techniques for the exploration and exploitation of geothermal energy: Università degli Studi di Genova, Genova, Italia, p. 30.

Mattson, E.D., Conrad, M.E., Neupane, G., McLing, T.L., Wood, T.R., and Cannon, C.J., 2016, Geothermometry mapping of deep hydrothermal reservoirs in southeastern Idaho: Final report: Idaho National Laboratory, Appendices B & C, p. 1-21.

Mazor, E., 1990, Applied Chemical and Isotopic Groundwater Hydrology: Halsted Press, New York, NY, p. 274.

McLing, T.L., McCurry, M., Cannon, C.J., Neupane, G., Wood, T.R., Podgorney, R., Welhan, J., Mines, G., Mattson, E.D., Wood, R., and Palmer, C., 2014, David Blackwell's forty years in the Idaho desert, the foundation for 21st century geothermal research: Geothermal Resources Council Transactions, v. 38, p. 143-151.

Mink, L.L., 2010, Camas Creek Ranch Geothermal Assessment Preliminary Report (unpublished).

Mitchell, J.C., 1976, Geothermal investigations in Idaho. Part 7. Geochemistry and geologic setting of the thermal waters of the Camas Prairie area, Blaine and Camas Counties, Idaho: Idaho Department of Water Resources, p. 3-25.

Nelson, S.T., 2000, A simple, practical methodology for routine VSMOW/SLAP normalization of water samples analyzed by continuous flow methods: Rapid Communication Mass Spectrometry, v. 14, p.1044-1046.

Neupane, G., Mattson, E.D., Spycher, N., Dobson, P.F., Conrad, M.E., Newell, D.L., McLing, T.L., Wood, T.R., Cannon, C.J., Atkinson, T.A., Brazell, C.W., and Worthing, W.C., 2017, Geochemical evaluation of the geothermal resources of Camas Prairie, Idaho, in Proceedings, 42nd Workshop on Geothermal Reservoir Engineering: Palo Alto, Stanford University, p. 12.

Nielson, D.L., and Shervais, J.W., 2017, Mafic heat sources for Snake River Plain geothermal systems, in Proceedings, 42nd Workshop on Geothermal Reservoir Engineering: Palo Alto, Stanford University, p. 8.

Parsons, T., Thompson, G.A., and Smith, R.P., 1998, More than one way to stretch: A tectonic model for extension along the plume track of the Yellowstone hot spot and adjacent Basin and Range Province: Tectonics, v. 7, p. 221-234.

Piper, A.M., 1944, A graphic procedure in the geochemical interpretation of water-analyses: American Geophysical Union Transactions, v. 25, p. 914-928.

Sanderson, B.M., and O'Neil, B.C., 2020, Assessing the costs of historical inaction on climate change: Nature, Scientific Reports, v. 10, article 9173.

Shervais, J.W., Shroff, G., Vetter, S.K., Matthews, S., Hanan, B.B., and McGee, J.J., 2002, Origin and evolution of the western Snake River Plain: Implications from stratigraphy, faulting, and the geochemistry of basalts near Mountain Home, Idaho, in Bonnichsen, B., White C.M., and McCurry, M., eds., Tectonic and Magmatic Evolution of the Snake River Plain Volcanic Province: Idaho Geological Survey Bulletin 30, p. 343-361.

Shervais, J.W., Schmitt, D.R., Nielson, D.L., Evans, J.P., Christiansen, E.H., Morgan, L., Shanks, P., Prokopenko, A.A., Lachmar, T.E., Liberty, L.M., Blackwell, D.D., Glen, J.M., Champion, D., Potter, K.E., and Kessler, J.A., 2013, First results from HOTSPOT: The Snake River Plain scientific drilling project, Idaho, U.S.A.: Scientific Drilling, v. 15, p. 36-43.

Shervais, J.W., Glen, J.M., Dobson, P.F., Gasperikova, E., Sonnenthal, E., Visser, C., Nielson, D.L., Garg, S.K., Evans J.P., Siler, D., DeAngelo, J., Athens, N., and Burns, E., 2015, Snake River Plain play fairway analysis – Phase 1 report: Geothermal Resources Council Transactions, v. 39, p. 761-767.

Shervais, J.W., Glen, J.M., Nielson, D.L., Garg, S.K., Dobson, P.F., Gasperikova, E., Sonnenthal, E., Visser, C., Liberty, L.M., DeAngelo, J., Siler, D., Varriale, J., and Evans J.P., 2016, Geothermal play fairway analysis of the Snake River Plain: Phase 1, in Proceedings, 41st Workshop on Geothermal Reservoir Engineering: Palo Alto, Stanford University, p. 6.

Shervais, J.W., Glen, J.M., Nielson, D.L., Garg, S.K., Liberty, L.M., Siler, D., Dobson, P.F., Gasperikova, E., Sonnenthal, E., Neupane, G., DeAngelo, J., Newell, D.L., Evans, J.P., and Snyder, N., 2017, Geothermal play fairway analysis of the Snake River Plain: Phase 2: Geothermal Resources Council Transactions, v. 41, p.14.

Shervais, J.W., Glen, J.M., Siler, D., Liberty, L.M., Neilson, D.L., Garg, S.K., Dobson, P.F., Gasperikova, E., Sonnenthal, E., Newell, D.L., Neupane, G., DeAngelo, J., Ritzinger, B., Peacock, J., Snyder, N., and Mink, L.L., 2018, Geothermal play fairway analysis, Phase 3: A provisional conceptual model of the Camas Prairie, Snake River Plain, Idaho: Geothermal Resources Council Transactions, v. 42, p. 11.

Smith, R.B., and Braile, L.W., 1994, The Yellowstone hotspot: Journal of Volcanology and Geothermal Research, v. 61, p. 121-187.

Smith, R.B., Jordan, M., Steinberger, B., Puskas, C.M., Farrell, J., Waite, G.P., Husen, S., Chang, W., and O'Connell, R., 2009, Geodynamics of the Yellowstone hotspot and mantle plume: Seismic and GPS imaging, kinematics, and mantle flow: Journal of Volcanology and Geothermal Research, v. 188, p. 26-56.

Strutt, R.J., 1906, On the distribution of radium in the earth's crust and on the earth's internal heat: Proceedings of the Royal Society of London, v. 77, p. 472-485.

Walton, W.C., 1962, Ground-water resources of Camas Prairie, Camas and Elmore Counties, Idaho: U.S. Geological Survey Water-Supply Paper 1609, p. 1-40.

White, D.E., 1968, Environments of generation of some basemetal ore deposits: Economic Geology, v. 63, p. 301-335.

Whitehead, R.L., 1992, Geohydrologic framework of the Snake River Plain regional aquifer system, Idaho and eastern Oregon: U.S. Geological Survey Professional Paper 1408-B, p. 1-29.

Williams, C.F., Reed, M.J., Mariner, R.H., DeAngelo, J., Galanis Jr., S.P., 2008, Assessment of moderate- and high-temperature geothermal resources of the United States: U.S. Geological Survey Fact Sheet 2008-3082, p. 1-4.

APPENDICES

Appendix A. XRD Results

| Table A.1. XRD Results. Minerals identified by the software appear before the ± those selected manually, after.		
Sample ID	Description	Mineralogy Results
8.C (B3, R6, 1635)	Dark w/ white phenocrysts ~3mm, vertical to 45 degree fractures w/ calcite mineralization each vein ~2mm thick	Quartz score: 49/scale factor: 0.937, Albite 38/0.600, Clinochlore (Chlorite) 33/0.200, Anorthoclase 25/0.179
A.1 (B4-R7-1643)	Salmon-colored granite	Quartz 43/0.377, Albite 28/0.474, Microcline 24/0.163, Laumontite (zeolite) 15/0.031
8.B (B4-R9-1655)	Chlorite chunk (green)	Quartz 54/0.529, Muscovite/illite 25/0.503, Epidote 28/0.045, Jacobsite 37/0.043
A.2 (B7-R14-1693)	Mafic dikelet, calcite veins, fractures running 65 degrees from horizontal, b/w granitic rocks	Quartz 65/0.907, Albite 37/0.217, Clinochlore 20/0.112, Gobbinsite 21/0.143
8.D (B7-R15-1696)	Granite Protolith – Kg – Idaho batholith	Quartz 59/0.335 Albite 37/0.262 Microcline 25/0.212
A.3 (B7-R15-1696.5)	Altered Granite	Quartz, Albite, Muscovite
A.4 (B12, R27, 1744)	Brecciated Granite	Quartz 53/0.430, Albite 33/0.575, Sanadine 21/0.186
A.5 (B12-R28-1746)	Andesite dikelet? Contact w/ granite above	Quartz 50/0.859, Calcite 47/0.210, Chlorite 25/0.092, Albite 35/0.316
A.6 (B15-R36-1775)	Green & red mineralized fracture, looks like chlorite	Quartz 41/0.254, Fe 45/0.072, Albite 24/0.715, Muscovite 23/0.100
8.A (B16-R37-1781)	Chlorite alteration/ Fe staining taken from fractured surface, Dip: near vertical split in core	Quartz 52/0.833, Albite 49/0.307, Muscovite 25/0.159, Philipsite (zeolite) 23/0.182 or Gobbinsite 18/0.090
A.7 (B22-R52-1851)	Mineralized surface, background granite, green, flaky	Quartz 49/0.600, Mica 42/0.051, Albite 31/0.388, Muscovite 28/0.134, Illite 24/0.129
A.8 (B26-R61-1889)	Red possible Fe-Staining, taken from fractured granitic surface	Quartz 47/0.922, Sanadine 24/0.293, Albite 22/0.178, Kaolinite 19/0.221, Muscovite 29/0.256
A.9 (B29-R69-1929)	Altered Granite	Quartz 50/0.859, Albite 40/0.298
A.10 (B31-R74-1946)	Altered rhyolite	Quartz 51/0.855, Albite 24/0.811, Chlorite 23/0.075, Muscovite 16/0.179, Microcline 24/0.247
A.11 (B32-R78-1971)	Rhyolite protolith	Quartz 52/0.983, Albite 31/0.222, Anorthoclase 14/0.134, Muscovite 20/0.228
A.12 (B34-R86-2002)	Altered chlorite, dip sub horizontal ~15 degrees	Quart 50/0.546, Albite 27/0.824, Illite 15/0.084, Anhydrite 21/0.046
A.13 (B35-R87-2007)	Granite/ Granodiorite, contact with rhyolite below	Quartz 52/0.592, Albite 31/0.348, Microcline 23/0.257, Calcite 26/0.079
A.14 (B36-R94-2024)	Rhyolite with mafics	Quartz 50/0.984, Microcline 26/0.258, Albite 28/0.291
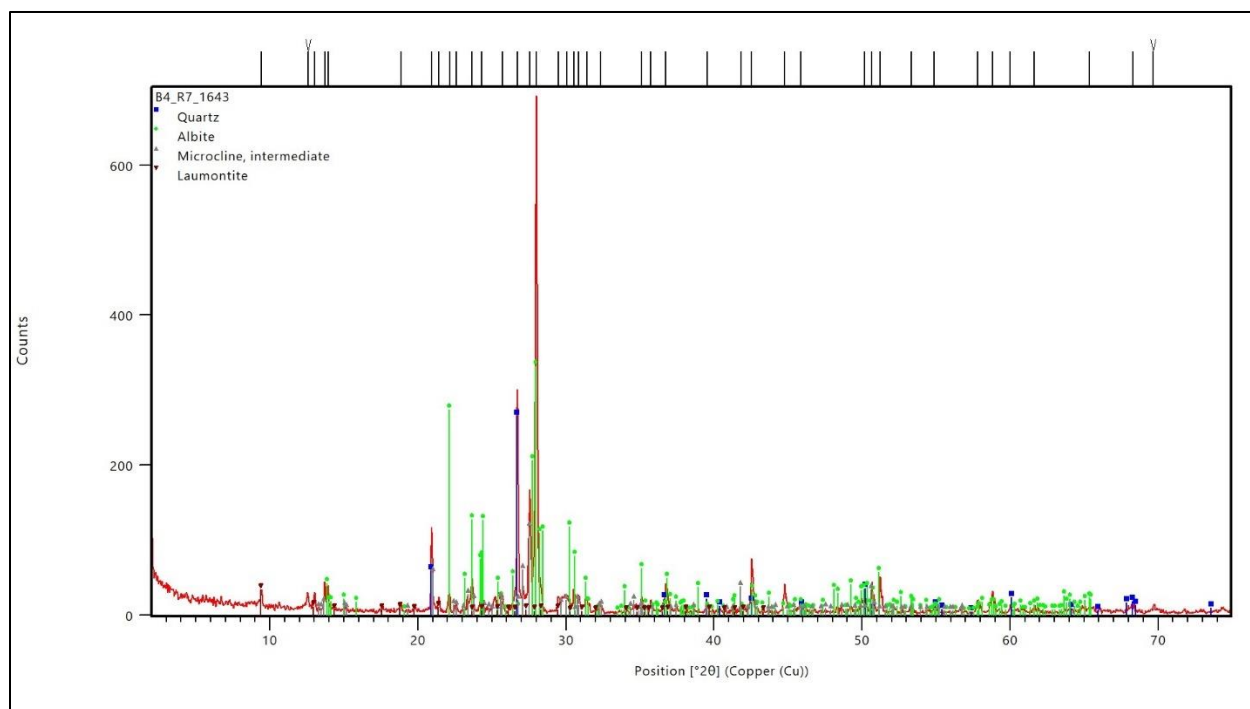
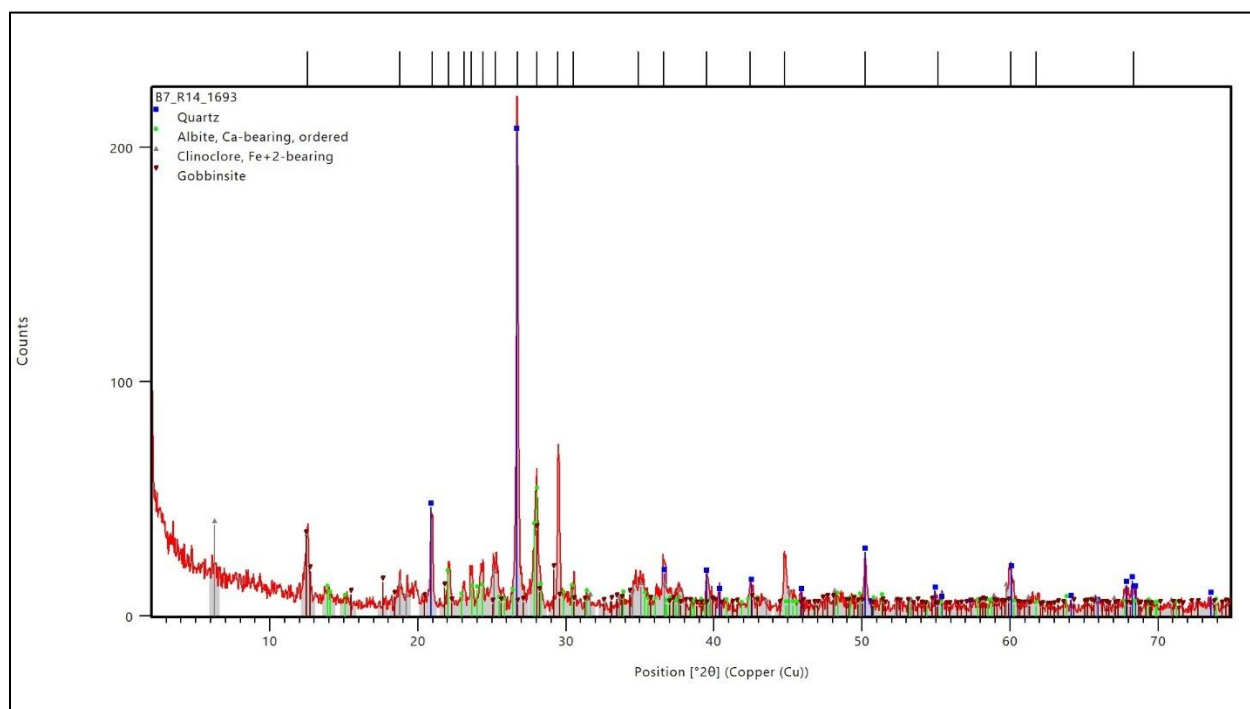Figure A.1. XRD diffractogram for sample B4-R7-1643, granite.

Figure A.2. XRD diffractogram for sample B7-R14-1693, mafic appearance w/ calcite.
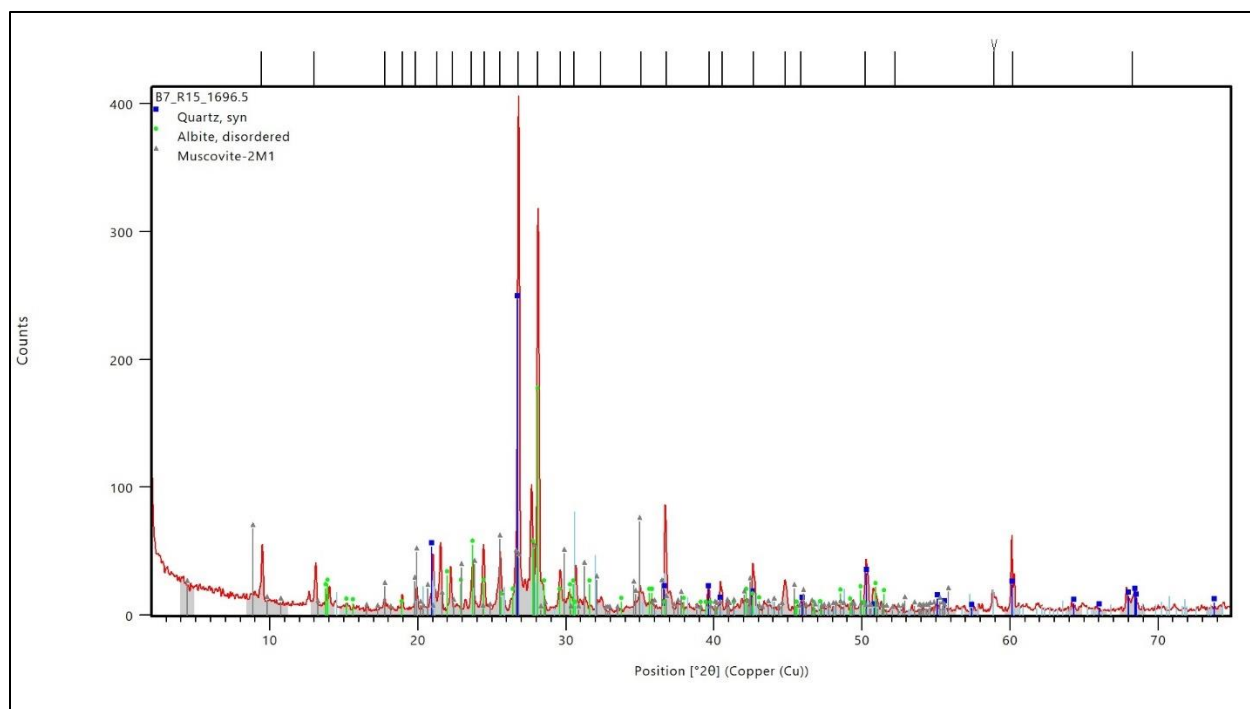
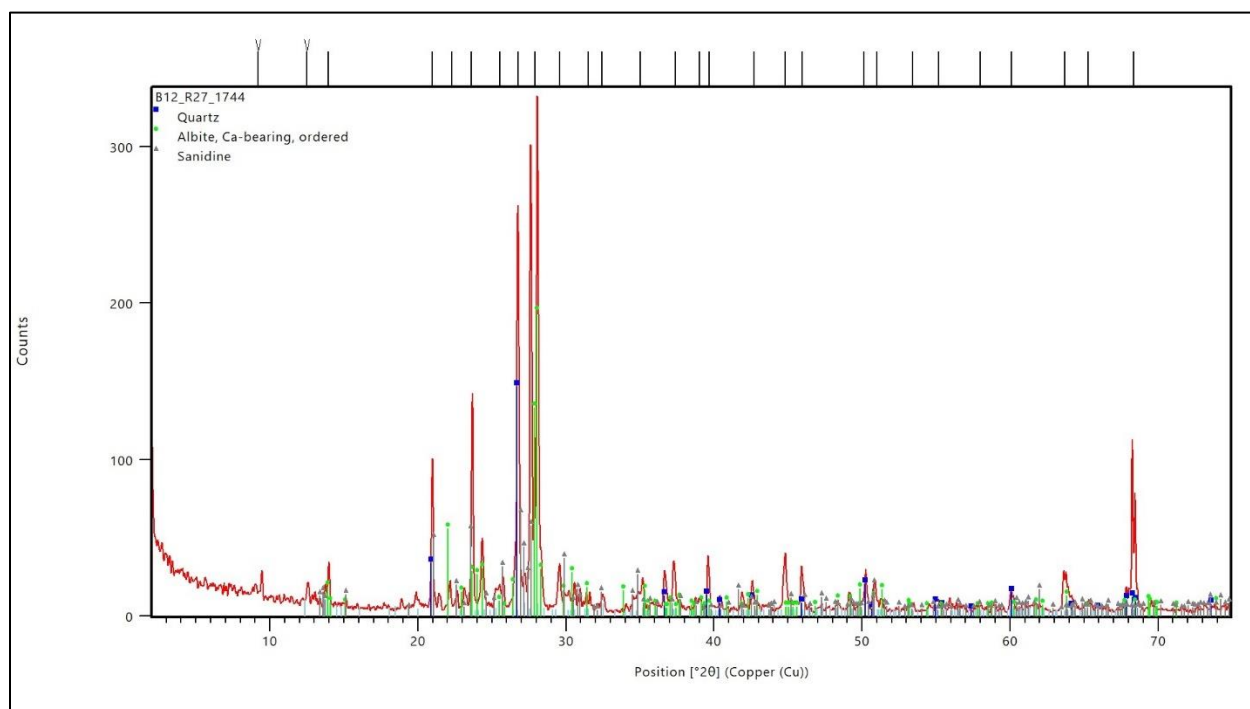Figure A.3. XRD diffractogram for sample B7-R15-1696.5, altered granite.

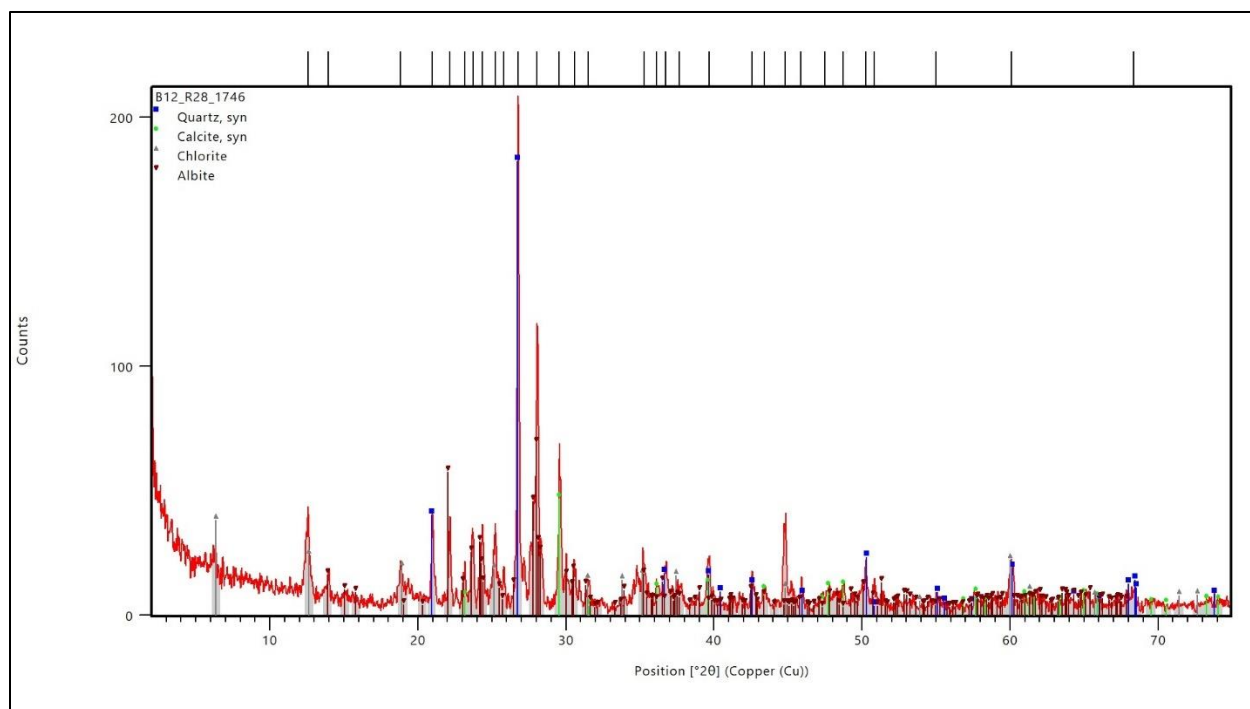Figure A.4. XRD diffractogram for sample B12-R27-1744, brecciated granite.

Figure A.5. XRD diffractogram for sample B12-R28-1746, intermediate to mafic appearance.
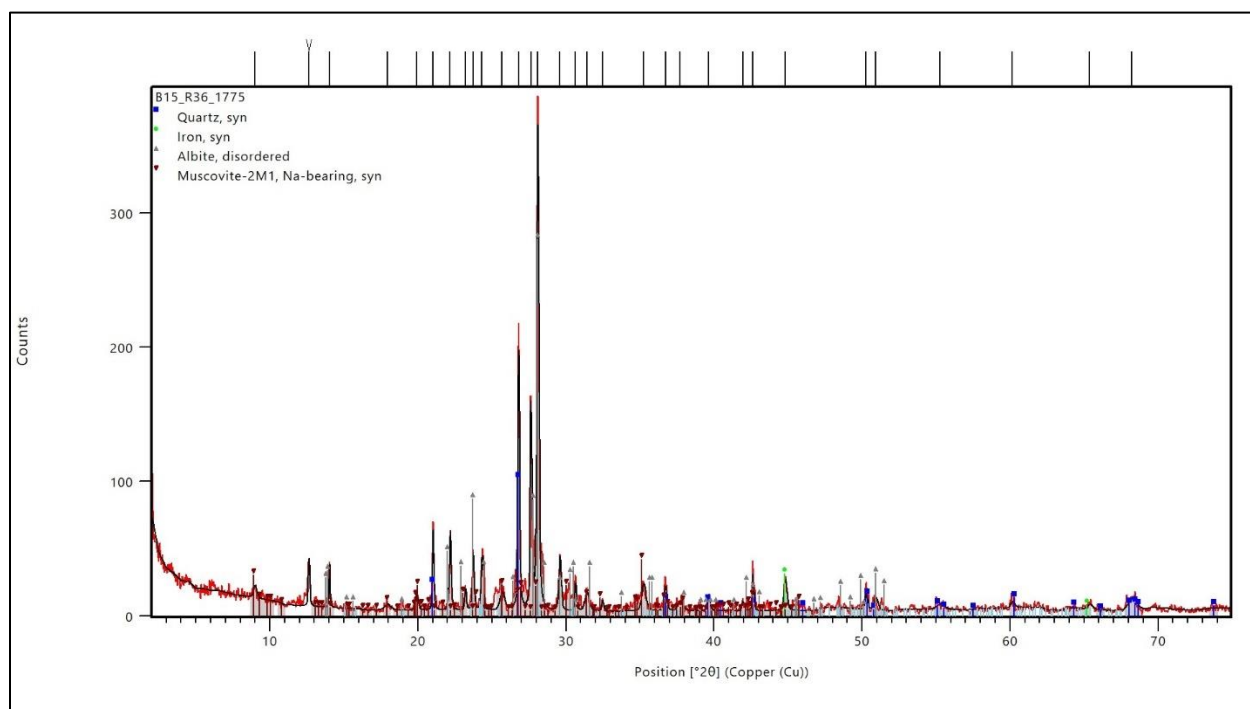

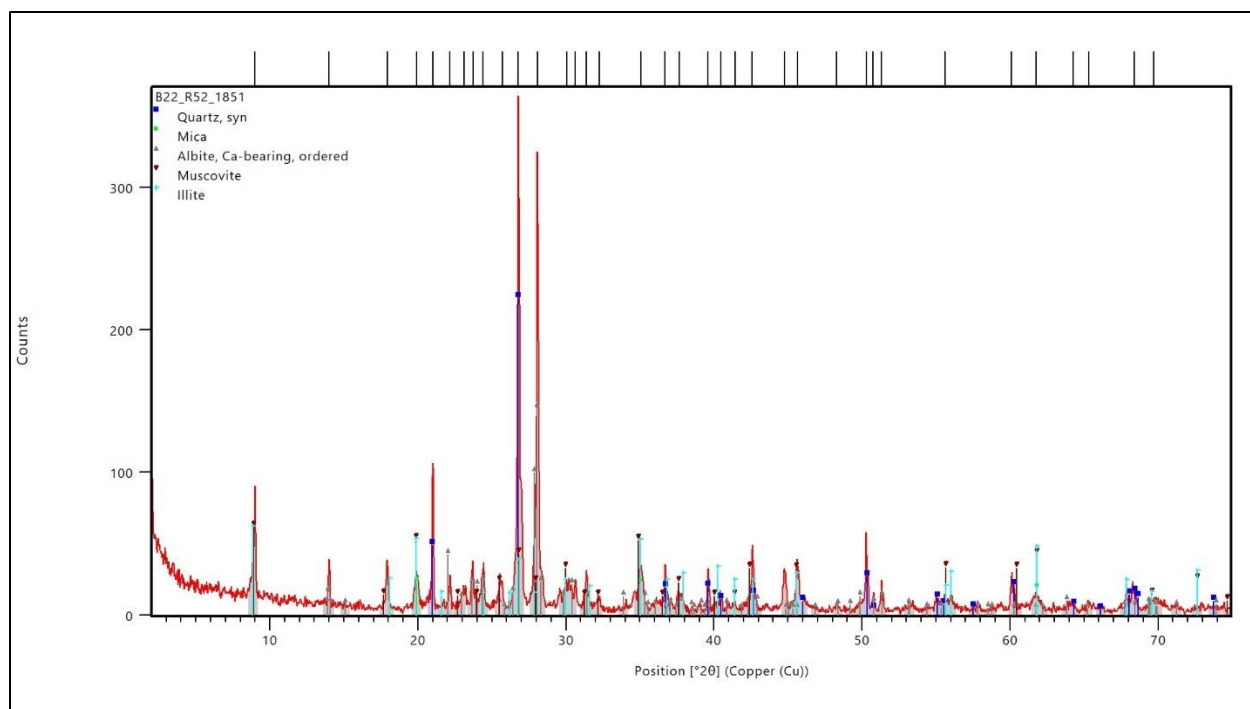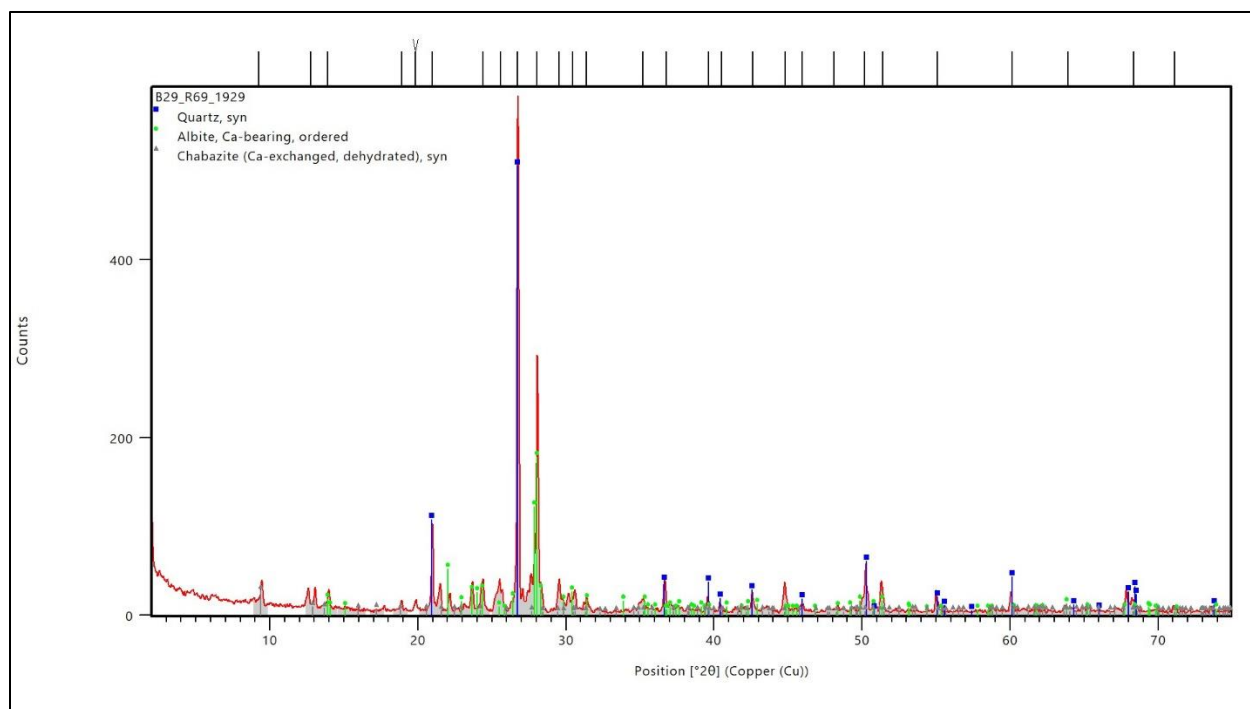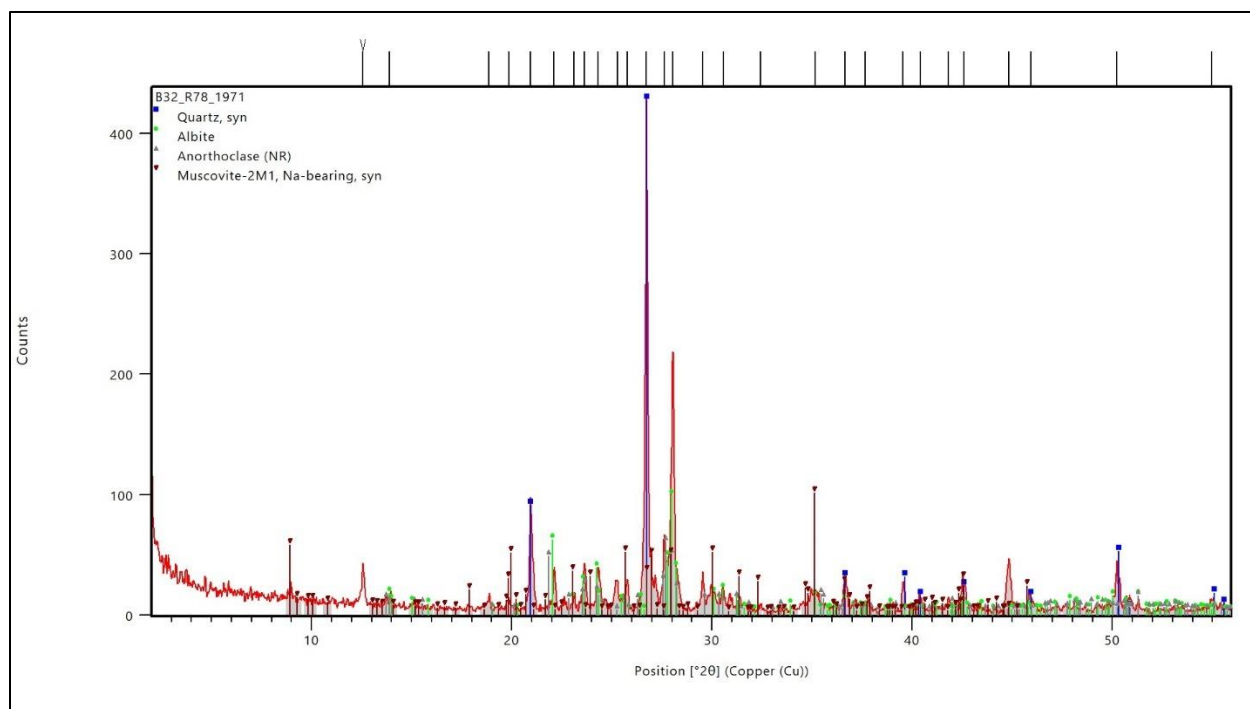Figure A.6. XRD diffractogram for sample B15-R36-1775, green and red mineralized fracture.

Figure A.7. XRD diffractogram for sample B22-R52-1851, mineralized granitic surface.
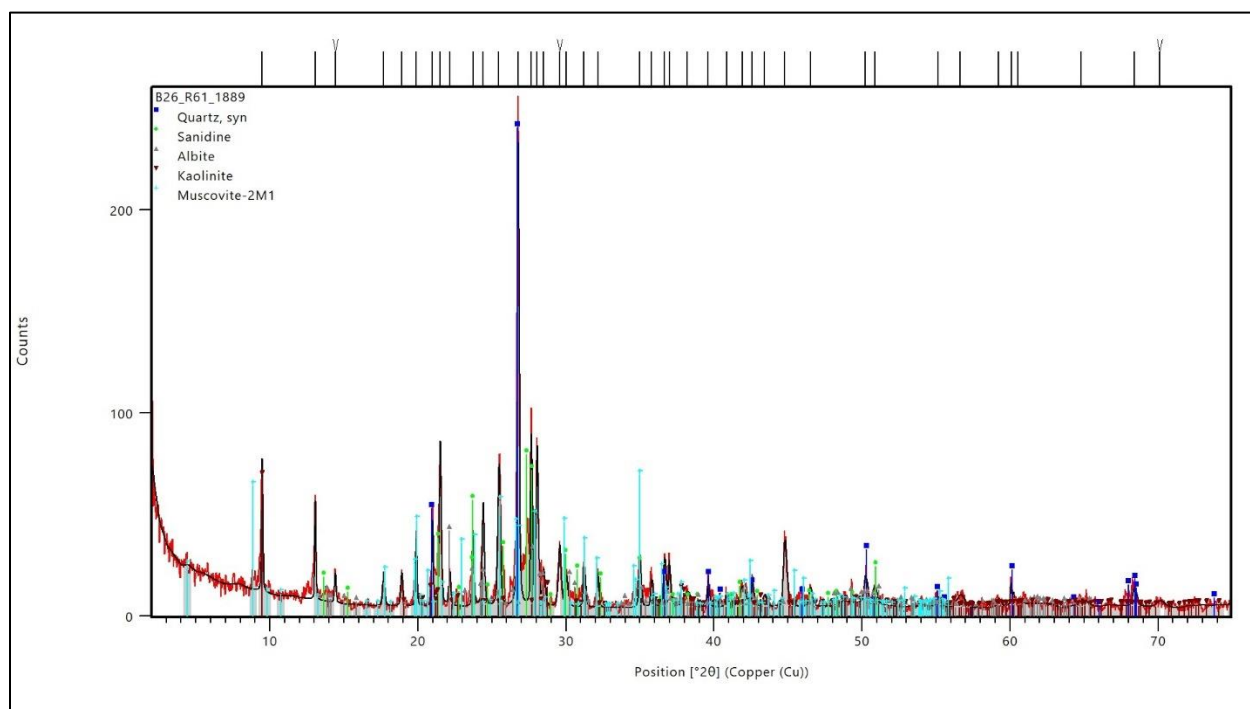
Figure A.8. XRD diffractogram for sample B26-R61-1889, red mineralized surface.

Figure A.9. XRD diffractogram for sample B29-R68-1929, altered granite.
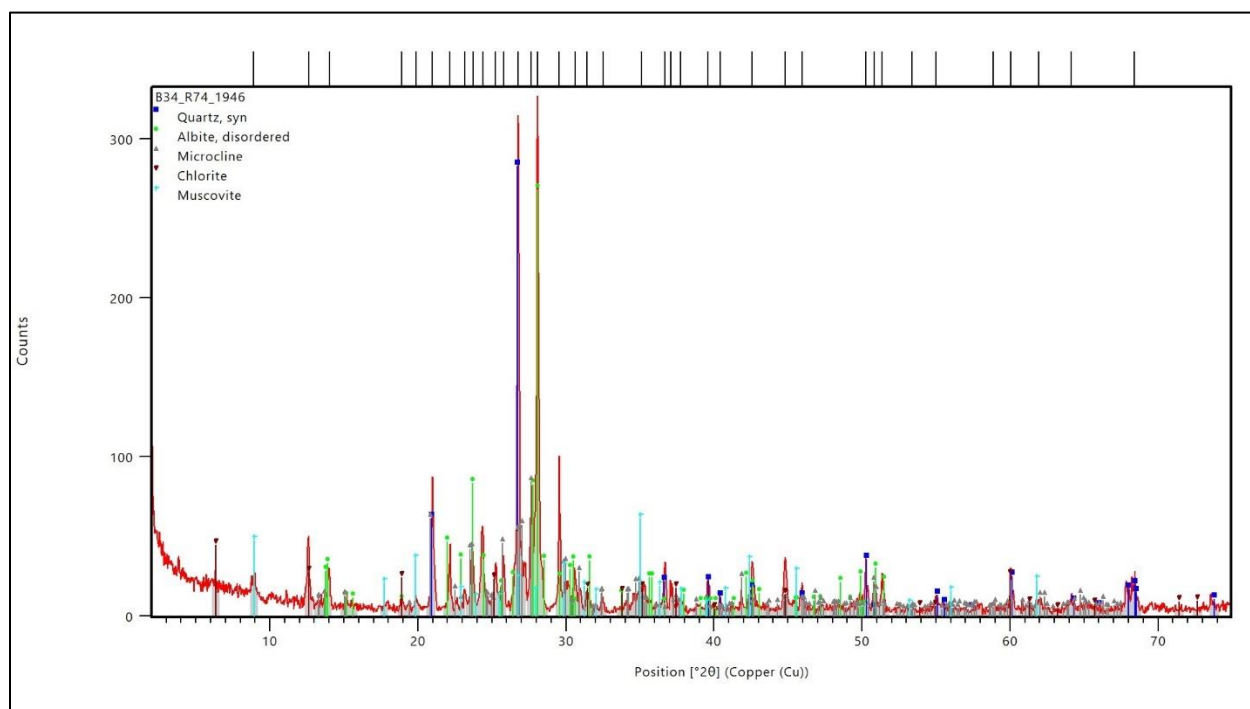
Figure A.10. XRD diffractogram for sample B29-R68-1946, altered granite.

Figure A.11. XRD diffractogram for sample B32-R78-1971, rhyolite protolith.
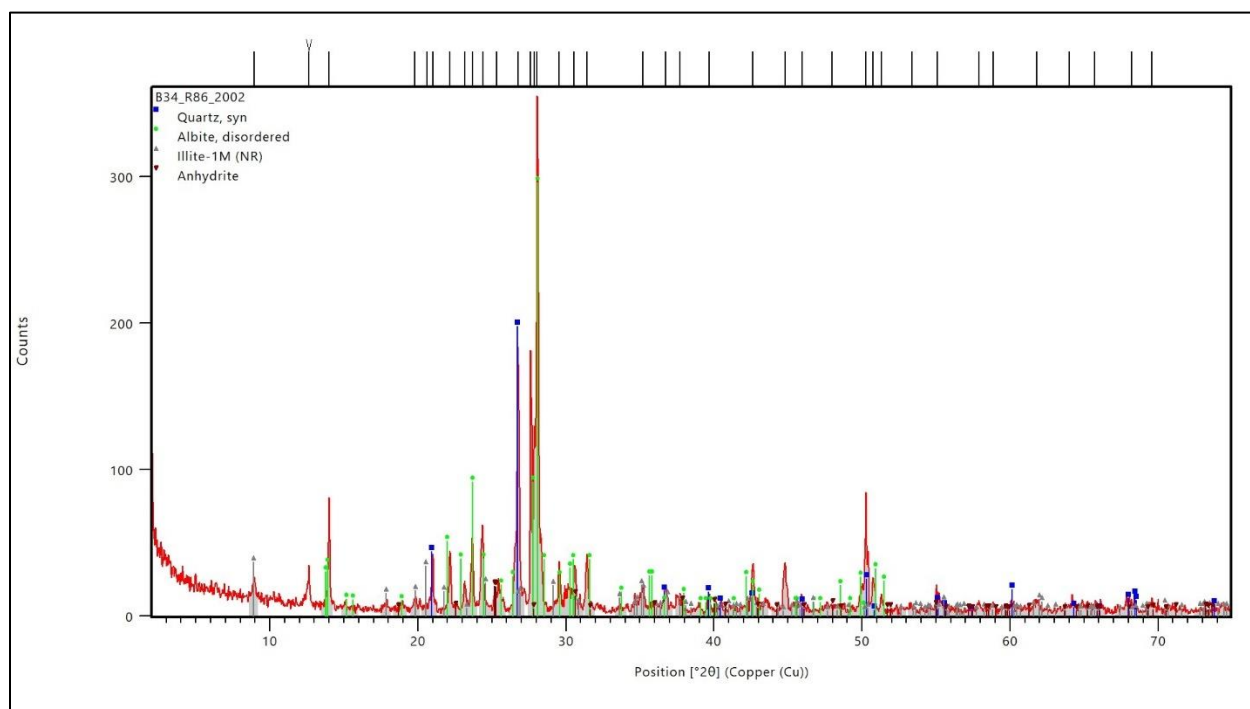
Figure A.12. XRD diffractogram for sample B34-R86-2002, green mineralized granitic surface.
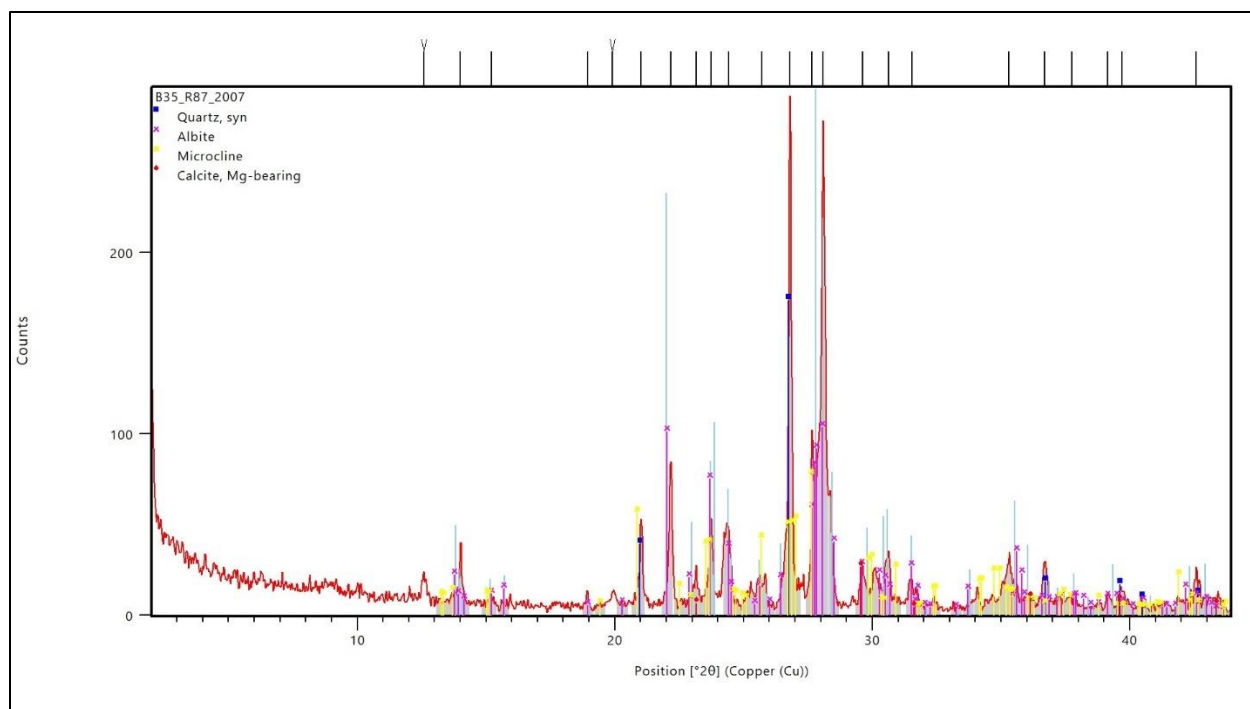
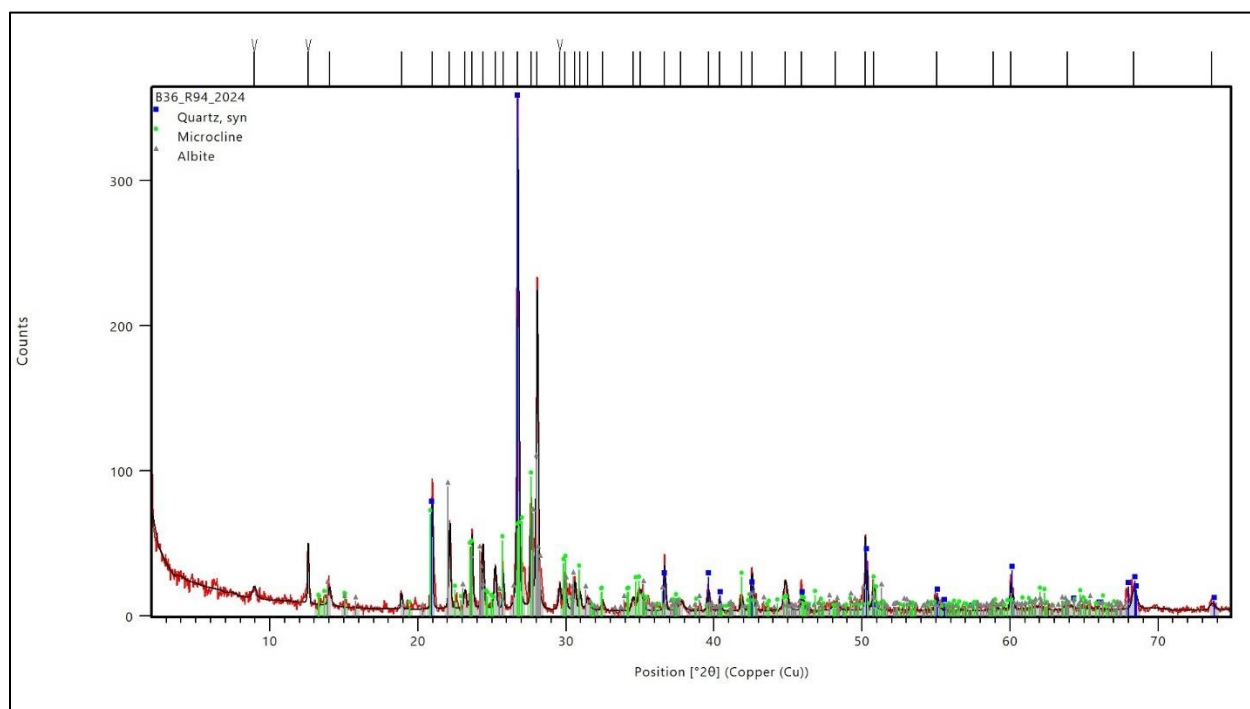Figure A.13. XRD diffractogram for sample B35-R87-2007, granite/granodiorite.

Figure A.14. XRD diffractogram for sample B36-R94-2024, rhyolite.

Appendix B. Chemical Results

Table B.1. USU Camas-1 chemical results (values in mg/L)		
Element	Camas	Detection Limits
Al	0.04	0.004
As	<	0.0002
Ba	0.22	0.001
Be	<	0.00003
Ca	2.29	0.08
Cd	<	0.00015
Cl	11.7	0.02
Co	<	0.00025
Cr	0.001	0.00005
Cu	<	0.0008
Fe	0.015	0.007
K	2.53	0.10
Mg	<	0.03
Mn	0.002	0.00015
Na	97.5	0.1
Ni	<	0.0004
P	<	na
Pb	<	0.00035
Sb	0.015	0.0024
Se	<	0.0001
Si	38.0	0.25
Sr	0.098	0.001
Ti	<	0.0001
V	<	0.00025
U	<	0.00006
Zn	0.026	0.0025

Note about ICP-MS and cations: helium was used to flush each sample except the barium, cadmium, antimony, barium, titanium, lead, and uranium samples (no gas).